Research Square

Preprints are preliminary reports that have not undergone peer review.
They should not be considered conclusive, used to inform clinical practice,
or referenced by the media as validated information.

# Modelling aboveground forest biomass as a continuous distribution using terrestrial and aerial laser scanning: a pathway to enhance the precision of forest biomass estimates

**Muluken N. Bazezew**

muluken.nega2025@gmail.com

University of Göttingen https://orcid.org/0000-0003-4440-1167

**Nils Griese**

University of Göttingen

**Thomas Seifert**

University of Freiburg

**Lutz Fehrmann**

University of Göttingen

**Christoph Kleinn**

University of Göttingen

**Nils Nölke**

University of Göttingen

**Research Article**

**Keywords:** Forest carbon stock, LiDAR point clouds, Plot level forest biomass aggregate, Remote sensing biomass prediction, Spatial distribution of crown biomass, Tree crown biomass

**Posted Date:** March 12th, 2026

**DOI:** https://doi.org/10.21203/rs.3.rs-9093008/v1

**License:** This work is licensed under a Creative Commons Attribution 4.0 International License.
Read Full License

**Additional Declarations:** The authors declare no competing interests.

# Modelling aboveground forest biomass as a continuous distribution using terrestrial and aerial laser scanning: a pathway to enhance the precision of forest biomass estimates

Muluken N. Bazezew [a, b, *], Nils Griese [a], Thomas Seifert [c], Lutz Fehrmann [a], Christoph Kleinn [a], Nils Nölke [a]

[a] Forest Inventory and Remote Sensing, University of Göttingen, Büsgenweg 5, 37077 Göttingen, Germany

[b] Department of Natural Resource Management, Debre Berhan University, Debre Berhan, P.O. Box 445, Ethiopia

[c] Forest Growth and Dendroecology, University of Freiburg, Tennenbacher Str. 4, 79106 Freiburg, Germany

*Corresponding author.

E-mail address: mbazeze@uni-goettingen.de; muluken.nega2025@gmail.com (M.N. Bazezew).

## Abstract

Estimating forest biomass and carbon storage is a core goal of many forest monitoring programs. Biomass assessments typically rely on allometric models to predict individual tree biomass from sample plots. Commonly, predicted tree biomass is then assigned exclusively to the stem position and fully added to a plot if the tree base lies within plot boundaries. However, tree biomass–particularly crown biomass–is spatially distributed across the crown projection areas. Consequently, crowns of trees inside a plot may extend beyond plot boundaries, while crowns of trees outside the plot may partially overlap the plot area. These boundary effects are not considered in conventional approaches during plot-level biomass aggregates–leading to errors when field-based biomass estimates are co-registered with remotely-sensed metrics, which provide continuous spatial signals at defined resolutions over tree canopies. The resulting scale-mismatch can compromise model qualities and increase uncertainty in remote sensing–based biomass predictions. Here, we further developed the 'horizontal biomass distribution (*HBD*)' approach–a solution that looks at the tree biomass strictly within the confinements

of the plot boundaries by spatially explicit modelling biomass as continuous horizontal distributions. We developed and evaluated two groups of *HBD* models using crown and point cloud metrics: **(1)** considering simplifying theoretical assumptions: perfectly upright stem, a circular crown projection area, and an isotropic biomass distribution around the stem axis; and **(2)** models accounting for stem irregularities, crown shape-asymmetries, and spatial biomass variabilities. The models were derived from point clouds generated by fusing terrestrial laser scanning (TLS) and unmanned aerial vehicle laser scanning (ULS) datasets. Our results show that integrating crown and point cloud metrics yields a more realistic representation of crown biomass distribution by capturing structural asymmetries and biomass variability. Point clouds provide a practical means for describing *HBD*, which would otherwise be impossible through direct measurements. The *HBD* is expected to improve biomass estimates by enabling a geometrically consistent linkage between plot-level biomass estimates and remotely-sensed metrics.

**Keywords:** Forest carbon stock; LiDAR point clouds; Plot level forest biomass aggregate; Remote sensing biomass prediction; Spatial distribution of crown biomass; Tree crown biomass

## 1. Introduction

Providing reliable estimates of forest biomass or carbon stock is among the core goals of most forest monitoring systems. Commonly, sample plot-level biomass is scaled up to the per-hectare biomass and to the whole forest inventory regions. The most basic element here is the plot-level biomass, which is determined by summing the complete individual tree biomass (typically predicted from allometric biomass models) of all sample trees counted within the inventory plots. In this commonly used approach, the total biomass of each tree is assigned exclusively to the corresponding tree stem position or geolocation – meaning that, in plot-level biomass aggregates, portions of trees extending beyond the plot boundary are not considered, and nor does it account for trees outside the plot have crowns that partially overlap the sample plot area (Fig. 1B). This does not represent the actual spatial distribution of biomass over the area defined by the crown projection, and is adequate for purely field sample-based estimates in forest inventory (Knapp et al., 2021; Mascaro et al., 2011). However, this approach would

be an error source when aggregated tree biomass estimates from field inventory plots are to be co-registered with ancillary metrics derived from remote sensing datasets, since biomass is realistically distributed across the crown projection area of individual trees, which is to be registered from above the tree canopies.

A potential solution beneficial to both field-based biomass estimates and remote sensing predictions is to model a close-to-realistic continuous distribution of biomass over the crown projection area of individual trees. Kleinn et al. (2020) and Pérez-Cruzado et al. (2021) introduce the concept of continuous distribution of forest biomass that allows cutting out the biomass exactly above the confinements of inventory sample plots (Fig. 1C). To model such a distribution of forest biomass, they modelled the '*horizontal biomass distribution (HBD)'* of individual trees and overlaid it on the inventory sample plots. Here, the crown biomass is modelled as a continuous distribution over the crown projection areas, so that the crown biomass can be determined for each section of the crown projection area of individual trees (Fig. 1C).

The *HBD* approach allows the total tree biomass of a specific plot to be aggregated in a geometrically explicit manner, exactly over the confinement of the corresponding plot boundary (Fig. 1C). This may prove relevant in enhancing remote sensing-based biomass prediction models (Kleinn et al., 2020), by offering to a more geometrically consistent alignment between plot-level biomass estimates and remotely sensed metrics. Further, the *HBD* approach may also be relevant when spatial distribution of forest fuel load should be modelled (Gale et al., 2021; Jiménez et al., 2013) – precise prediction of fuel load is essential for assessing forest fire risks and behaviours, especially in the context of high-intensity crown fires that spread vertically and horizontally through the canopy rather than the forest floors. In such cases, the *HBD* approach may be used in reliable prediction of the spatial distribution and density of canopy fuels, which directly influence fire spread and intensity, thereby enabling researchers and foresters to obtain a spatial profile of biomass or combustible materials across the horizontal sections of tree crowns. The *HBD* approach may also be applicable in forestry, where estimating the proportion of biomass loss from partially snapped tree crowns (Hall et al., 2020; Zuleta et al., 2022) is of interest.

For example, in cases when trees have partially damaged crowns due to storms, mechanical harvesting, or other disturbances, the approach allows for more spatially explicit estimation of biomass losses.

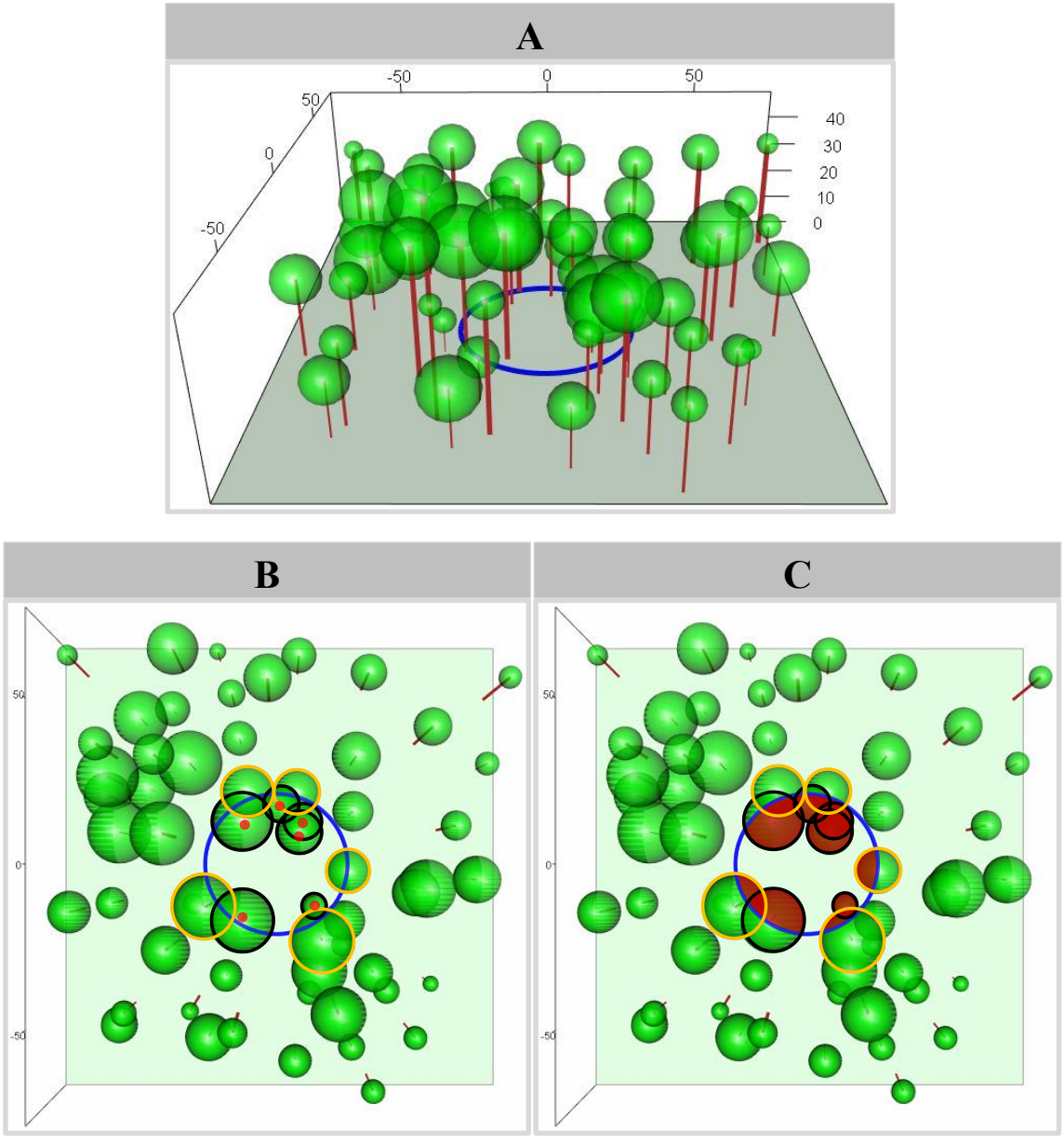



**Fig. 1.** Comparison of traditional and *HBD* approaches for estimating tree biomass. (A) Forest stand with an inventory plot (blue); (B–C) horizontal projections. Black circles mark crowns of trees with stems inside the plot, and orange circles mark crowns extending from outside. (B) Traditional approach: only trees with stems inside the plot are included, with overall tree biomass assigned to the corresponding stem position (red points). (C) *HBD* approach: biomass within the plot is estimated based on crown areas intersecting the boundary, represented as a continuous horizontal distribution of

87 individual tree biomass over the area defined by the crown projection (red areas). The circular crowns
88 and uniform *HBD* shown are simplified illustrations.

89 Unlike the vertical crown biomass distribution (Tahvanainen and Forss, 2008; Ver Planck and
90 MacFarlane, 2014; Zuleta et al., 2022), approaches to model the *HBD* are rare in the forestry research
91 (Pérez-Cruzado et al., 2021). Methodological gaps and data acquisition techniques characterizing crown
92 architectures have further hindered the development of comprehensive *HBD* descriptions. Pérez-
93 Cruzado et al. (2021) described *HBD* from field or direct measurements (on a sample of small dimension
94 beech trees, *Fagus sylvatica*, with single upright trunks and no stem irregularities), which proved to be
95 highly laborious, requiring felling of trees, and measurement of branch biomass from multiple sections.
96 This method requires measuring the angle of the branch sections to project the biomass onto a horizontal
97 plane, making it impossible for larger trees. For practical reasons, they made simplifying assumptions,
98 such as primary branches are to be perfectly straight, and having a constant angle of inclination along
99 the entire length of the corresponding branches. Furthermore, it was assumed that all higher-order
100 branches lie in the same plane as the primary branch's inclination angle, which does not hold true in
101 reality, especially for large tree crowns. The previous *HBD* models (Bazezew et al., 2024a; Pérez-
102 Cruzado et al., 2021) were also developed based on certain simplifying theoretical assumptions, such
103 as the trees standing perfectly upright, the crown projection area of trees being circular, and the
104 corresponding biomass being isotropically distributed around the stem axis – all of which do not reflect
105 the actual tree stem and crown structures, particularly in larger trees. To date, no robust approach has
106 been developed for observing the *HBD* that explicitly accounts for stem irregularities, crown shape
107 asymmetries and associated biomass variability across the crown parts of individual trees.

108 In this research, the crown biomass proxies used for modelling of the *HBDs* were derived by a
109 complete reconstruction of three-dimensional tree models based on high-resolution tree point clouds
110 obtained from a fusion of terrestrial laser scanning (TLS) and unmanned aerial vehicle laser scanning
111 (ULS) datasets. Point clouds enable non-destructive three-dimensional characterization of forest
112 structures, promoting accurate retrieval of crown metrics (Panagiotidis et al., 2022; Qi et al., 2022;
113 Terryn et al., 2022) while avoiding labour-intensive fieldwork and inconvenient direct measurements.

Several studies have used LiDAR point clouds, such as from ULS and TLS techniques, to estimate tree biomass and crown metrics and found close agreement with destructive measurements (Calders et al., 2015; Momo Takoudjou et al., 2018; Qi et al., 2022). However, the accuracies rely on point cloud characteristics, such as point density and occlusion levels (Hackenberg et al., 2015; Momo Takoudjou et al., 2018; Raumonen et al., 2013), where the point characteristics are influenced by tree dimensions, crown architecture, presence of foliage, scanning positions and distances, and wind conditions (Dassot et al., 2011; Griebel et al., 2015; Li et al., 2020). This has been shown to be critical, principally for the upper parts of large tree crowns and finer branches – with any geometric approximation techniques including voxelization (Hosoi et al., 2013), laplacian contraction algorithm (Li et al., 2020), hull modelling (Stovall et al., 2017), and quantitative structural modelling (QSM) (Hackenberg et al., 2015; Morhart et al. 2024; Raumonen et al., 2013). Therefore, to reduce uncertainties, the *HBD* modelling approaches using point clouds should also be robust to the typically deficient datasets.

The integrative use of TLS and ULS datasets enhances point cloud completeness and density from ground to the forest canopies (Bazezew et al., 2018; Dai et al., 2019; Qi et al., 2022), enhancing the accuracy of crown metrics and volume estimates (Panagiotidis et al., 2022; Weiser et al., 2022; Zhou et al., 2023). In this study, TLS provided high-resolution laser returns across the lower to upper crown sections of individual trees, with reflection quality affected by branch occlusion and tree dimensions, resulting in denser points in the lower- and middle-crown sections. Complementarily, ULS enhanced point cloud quality by capturing a higher number of lasers returns from the upper canopy regions. The combined ULS and TLS datasets have, therefore, enabled the production of comprehensive three-dimensional reconstructions of the complete tree crowns, offering robust spatial distribution of crown biomass proxies – which would otherwise be impractical to obtain through direct measurements.

The overall aim of this research was to develop *HBD* models that describe the spatial distribution of crown biomass over the area defined by the horizontal projection of individual trees. Specifically, the objectives addressed in this study comprise: (**1**) to develop a non-destructive methodology to describe crown biomass as a continuous distribution from point clouds; and (**2**) to evaluate various operational empirical functions and theoretical considerations used to provide a near-realistic description of the

*HBD* of individual trees, also by accounting for stem irregularities, crown shape asymmetries and biomass variability across crown parts.

## 2. Materials and methods

### *2.1. Study area and data source*

We collected TLS and ULS data at the sites of a long-term research programme of the German Research Foundation, DFG (Exploratories for Large-Scale and Long-Term Functional Biodiversity Research - Biodiversity Exploratories, SPP1374) (Fischer et al., 2010). The sites were located within three regions in Germany: Schorfheide-Chorin Biosphere Reserve (SCH) in north-eastern Germany; Hainich-Dün (HAI) in central Germany; and Schwäbische Alb (ALB) in south-western Germany (Fig. 2).

The TLS datasets were acquired using a Leica BLK360 G1 laser scanner (Leica BLK360 G1 Imaging Laser Scanner, 2024) during leaf-off conditions between January 2023 and March 2023. The Leica BLK360 G1 is a high-speed time-of-flight scanner operating in the near infrared spectrum (830 nm) with a beam divergence of 0.4 mrad and an acquisition rate of 360,000 pts.s$^{-1}$. The BLK360 G1 is a lightweight scanner (1 kg) with an accuracy of ±6 mm at 10 m and ±8 mm at 20 m, and a maximum scanning range of 60 m. More details of the sensor are shown in Table 1. The TLS data were collected from five scan positions positioned around the plot center and perimeter of the circular plot design (approximately 45 m radius) at the Biodiversity Exploratory (BE) sites of the *FOrest Gap eXperiment (FOX)*. The design of the *FOX* plots is described in Fischer et al. (2010). For higher point cloud densities in the vicinity of tree crowns, two consecutive TLS scans were performed at the perspective scan positions: low-tripod scan (scanning with a tripod ≈2 m above the ground) and high-tripod scan (scanning with a tripod ≈8 m above the ground). For a high-tripod scanning, the scanner was mounted on a tall telescopic tripod from Bernhardt Media Solutions (https://www.hochstativ.de/), which reaches a maximum height of 10 m when fully extended. The scanning setup and procedure is found in Griese et al. (2025). The ULS datasets were acquired concurrently with the TLS scans using a Phoenix

RECON-XT LiDAR sensor mounted on a DJI Matrice 350 drone (RECON-XT LiDAR, 2024). The RECON-XT is also a time-of-flight laser sensor operating at a wavelength of 905 nm with a beam divergence of 1.52 mrad. The sensor has a laser acquisition rate of 640,000 pts.s$^{-1}$ at a maximum range of 120 m. See Table 1 for further details. The point cloud data was collected by flying the drone at an average survey altitude of 80 m above ground with an average flight speed of 6 m.s$^{-1}$; offering ≈1,900 pts.m$^{-2}$.

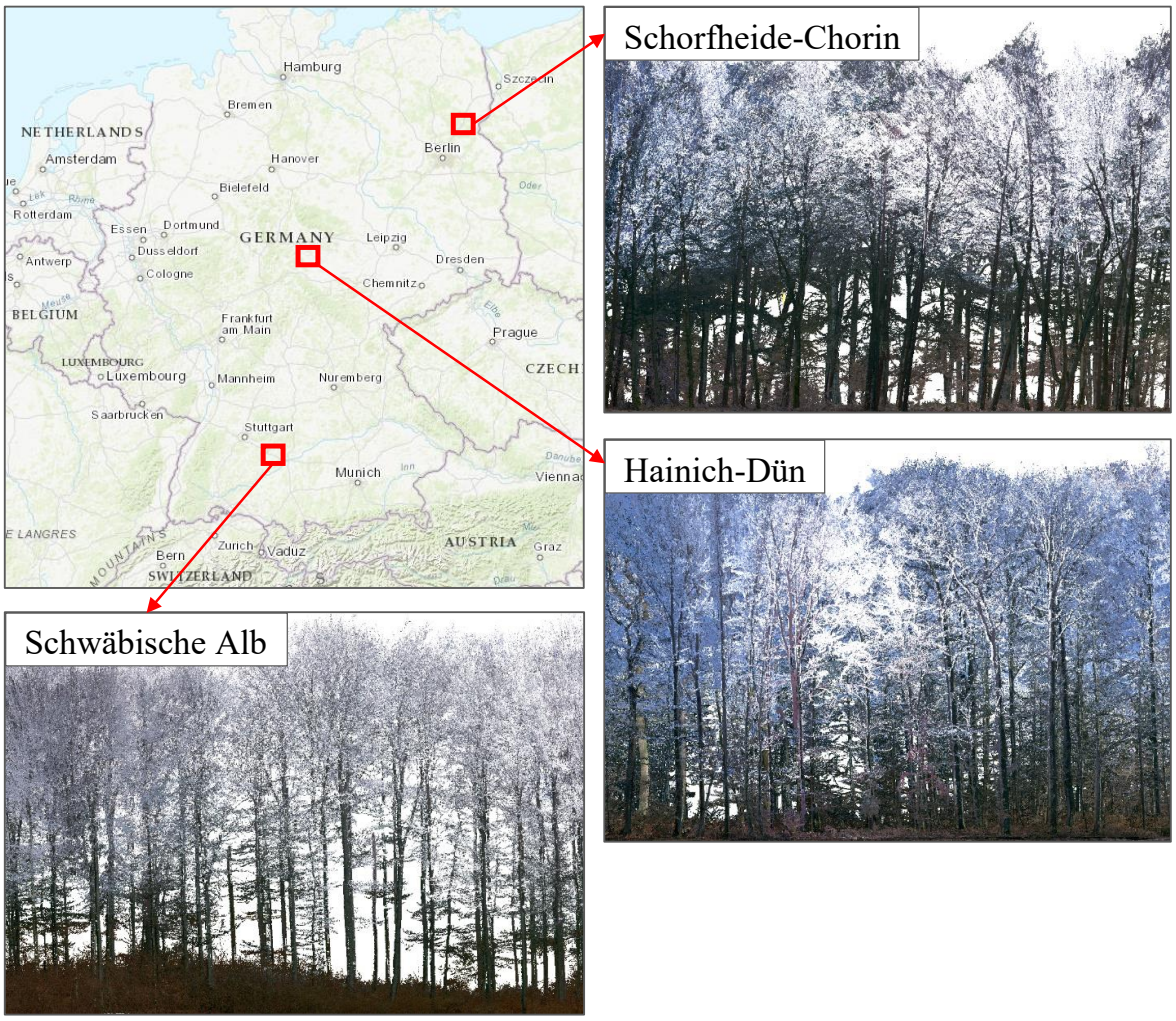



**Fig. 2.** Geographic location of our study sites within the Biodiversity Exploratories, highlighted with a sample of TLS scan point clouds (RGB colour) each.

**Table 1.** Specification of the TLS (Leica BLK360 G1 LiDAR) and ULS (with RECON-XT LiDAR sensor)

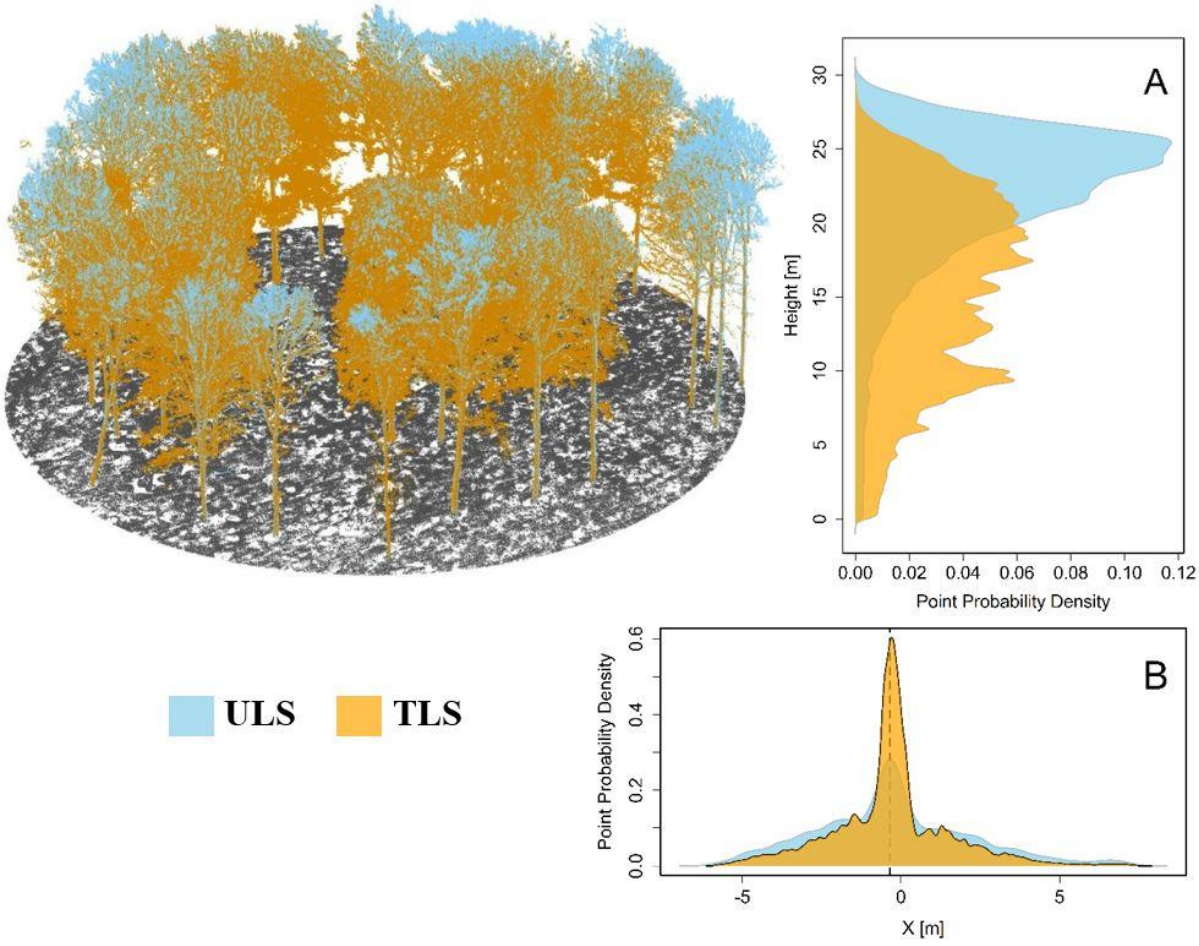
| Specification | TLS - Leica BLK360 G1 laser scanner | ULS with RECON-XT LiDAR sensor |
|---|---|---|
| Accuracy | 6 mm at 10m; 8 mm at 20m | 10 mm within 0.5 – 70 m |
| Measuring range (m) | 0.6 – 60 | Max. 120 |
| Wavelength (nm) | 830 | 905 |
| Scanning field-of-view | 300° V / 360° H | +15° -16° V / 360° H |
| Point measurement rate (pts.s$^{-1}$) | ≈360,000 | 640,000 |
| Beam divergence (mrad) | 0.4 | 1.52 |
| Pulse repetition frequency | 1.44 MHz | 640 kHz |
| Operating temperature (°C) | +5 – +40 | –20 – +40 |
| Weight (kg) | 1 | 1.8 |
| Dust/Humidity | Solid particle/ liquid ingress protection | |
| Remote operation | Cyclone field 360 Compatibility | |
| Wireless communication | Integrated wireless LAN | |
| Tripod height | Low (2 m), and high (Max. of 10 m) | |
| Constellation Support | | GPS, GLONASS, BEIDOU, GALILEO |

### *2.2. TLS and ULS data processing, and single tree extraction*

Co-registration of all TLS scan positions was performed using Leica Cyclone Register 360 Plus software, version 2024.0.1 (Cyclone Register 360 Plus, 2024). A cloud-to-cloud registration method was applied by supervised visual detection of overlapping points; followed by fine-registration using the iterative closest point (ICP) algorithm – implementation in Leica Cyclone software. Registration quality was checked using the 'TruSlicer' tool in the same software, where samples of trunk points were sliced and checked until no edge offset was observed between point clouds from all scanning positions. The point clouds were normalized using lidR package, version 4.1.0 (Roussel et al., 2024), implemented in the R programming language (R Core Team, 2024). We removed point cloud artifacts ($z < 0$ and $z >$ 50 m), considering the ground level and maximum height of the trees across the study sites. Further, we filtered the noise in the point cloud using statistical outlier filtering in CloudCompare software, version

188 2.13.0 (CloudCompare, 2024). Here, we set two parameters: the number of neighbouring points as the
189 mean distance estimate (*n*), and the standard deviation multiplier threshold (*k*). We set *n* between 4 and
190 10 (depending on the noise level of the scan plots), while *k* was fixed at 1.0. The ULS datasets were
191 processed using Phoenix LiDARMill software, version v3 (LiDARMill, 2023). The point clouds were
192 classified as ground and non-ground returns using the progressive triangular network method (TIN)
193 (Lindberg et al., 2012), where the canopy height model (CHM) is computed based on these point clouds.
194 Likewise, the outliers from the ULS dataset were eliminated from the normalised point clouds based on
195 the ground level and maximum canopy height values of the trees ($z < 0$ and $z > 50$ m).

196 The normalized point clouds from the TLS and ULS were then clipped to 45 m radius from the
197 center of the plots (Fig. 3). The two datasets were fused using CloudCompare software (CloudCompare,
198 2024) (Fig. 3). The two data sources were aligned by cloud-to-cloud matching through supervised visual
199 inspection of the overlapping tree points. Initially, coarse alignment was performed using the manual
200 coarse alignment (Translate/Rotate tool), where the ULS cloud was manually adjusted to visually match
201 the TLS reference clouds. Then, fine registration was executed using the ICP algorithm, configured
202 with a point-to-point distance metric, overlap of 99%, and with a maximum of 50 iterations –
203 implemented in the same software. The final alignment produced a maximum overlap root mean square
204 error of 0.06 m, which can result in insignificant discrepancies in the determination of tree metrics, as
205 also reported in Li et al., (2020) and Pitkänen et al., (2021). The fused TLS-ULS datasets provided laser
206 points across individual tree parts: TLS contributed greater point density in the lower and mid-crown
207 regions, while the ULS improved laser hits in the upper crown parts, as shown in Fig. 3. This allows
208 for a better complete tree crown reconstructions (Section 2.3.1).




209

210 **Fig. 3.** TLS and ULS fused point clouds of a sample plot. After excluding ground points (grey points),
211 the datasets contain the following number of points: ULS = 1.17 million pts (287 pts.m$^{-2}$), TLS = 56.95
212 million pts (11, 707 pts.m$^{-2}$); and the fused point clouds = 58.12 million pts (13, 121 pts.m$^{-2}$). The
213 corresponding point density plots are shown: (A) point probability density vertically over tree height;
214 and (B) horizontal point probability density. The TLS-based point density is higher toward the lower
215 parts of the crowns and trunks, while the ULS provided higher point density around the upper parts of
216 the tree crowns.

217 The single tree segmentation was executed using the TreeLearn package implemented in Python,
218 version 3.9.19 (TreeLearn, 2024), example shown in Fig. 4. TreeLearn is a deep learning approach of
219 tree instance segmentation of forest point clouds (Henrich et al., 2024). After visual inspection of
220 individual tree segments, unsuccessful segments were excluded from further derivation of crown
221 biomass and determination of tree metrics. Undergrowth vegetation, such as segmented points of
222 regeneration trees, shrubs, and herbs were also excluded from the biomass assessments. The scanned

plots were dominated by European beech (*Fagus sylvatica*) trees. A few other tree species, such as oak (*Quercus robur*), European ash (*Fraxinus excelsior*), Norway maple (*Acer platanoides*), Scots pine (*Pinus sylvestris*), and Norway spruce (*Picea abies*) were also found. Due to the challenges and uncertainties of crown reconstruction, we excluded coniferous tree species from further analysis. The dimensions of the sample trees are shown in Fig. 5. The determination processes the tree dimensions and further model input variables are described in Table 2.

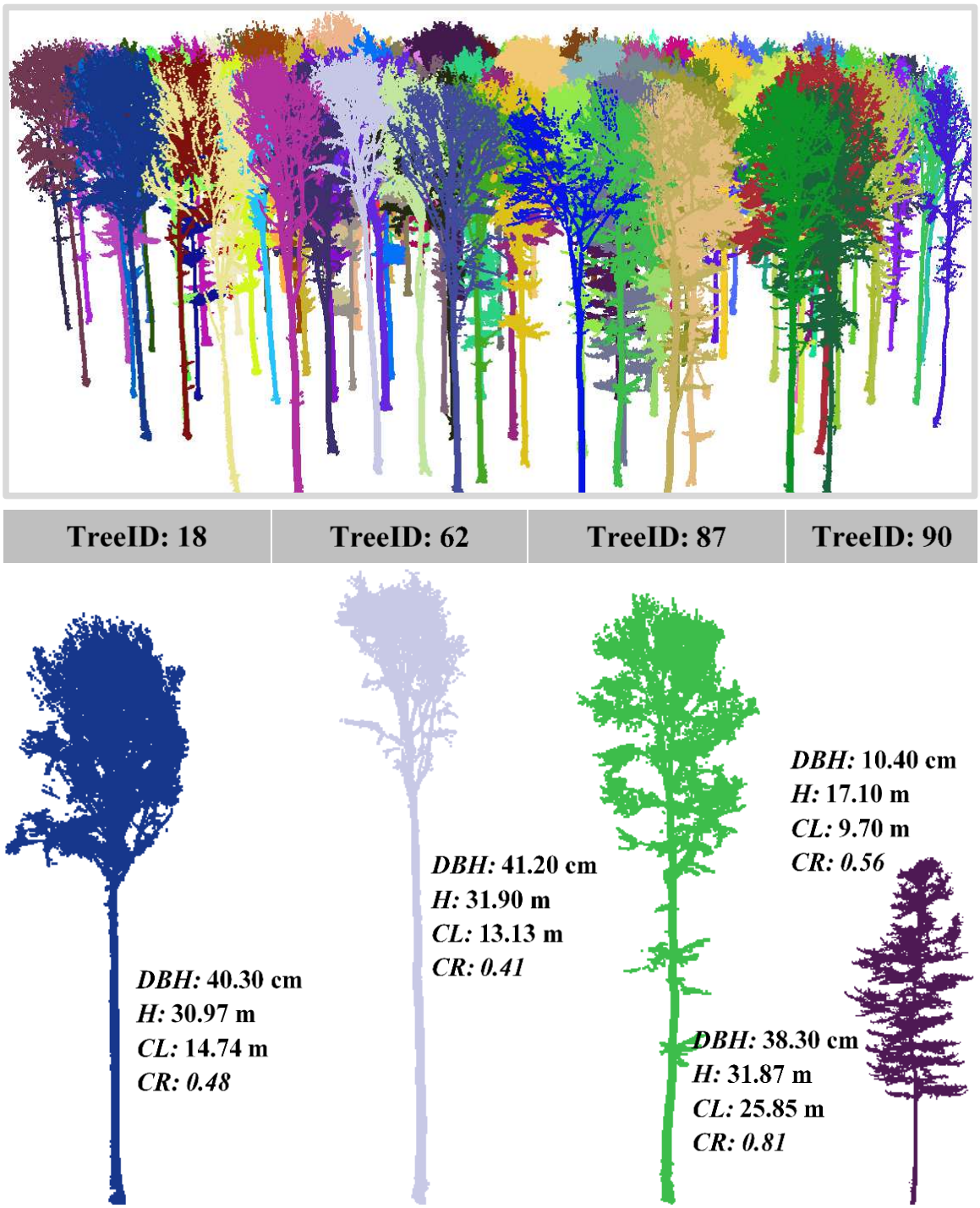


**Fig. 4.** 119 trees extracted from a sample of a plot using an automated segmentation method. The corresponding isolated trees (bottom) with variables, such as diameter at breast height (*DBH*), tree height (*H*), crown length (*CL*), and crown ratio (*CR*), determined directly from the laser points, based on as described in Table 2.

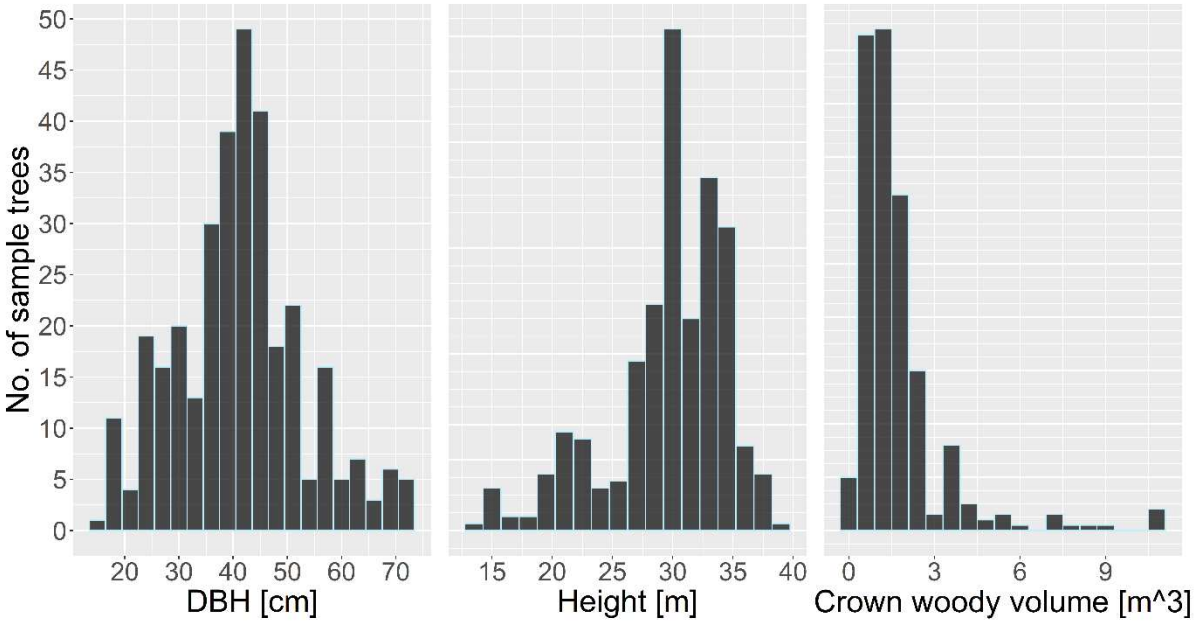



**Fig. 5.** Diameter, height, and crown volume distribution of scanned sample trees. The bin sizes are 3 cm, 1.5 m, and 0.2 $m^3$ for tree diameters, heights, and volumes, respectively.

### *2.3. Modelling horizontal biomass distributions (HBDs) and extraction of model input variables*

#### *2.3.1. Crown woody biomass proxies from point cloud data*

A proxy for crown biomass was determined using quantitative structural modelling (QSM) (Hackenberg et al., 2015). In this study, we employed plot-based QSM reconstructions with the fused point clouds using the Computree platform, version v5.0 (Computree, 2024) through a SimpleForest plugin, version 5.3.2 (SimpleForest, 2024) (Fig. 6). We first generated fitted cylinders using a basic sphere-following the algorithm of Hackenberg et al. (2015) and the maximum likelihood estimation sample consensus algorithm, MLESAC (Torr and Zisserman, 2000). To improve the quality of the cylinder fits, we further applied the shoot and allometric correction algorithms (Hackenberg et al., 2015).

The results of the QSM cylinder fits were manually evaluated by comparing the QSM with the original point clouds. For trees with substantial noise and occlusion caused by extensive branch interlocking, the reconstructions were significantly affected, leading to the loss of large portions of the crown; as also reported in many studies (Bazezew et al. 2024b; Calders et al., 2015; Demol et al., 2022; Hackenberg et al., 2015; Lau et al., 2018; Raumonen et al., 2013). These trees were excluded from subsequent spatial biomass distribution modelling process. In total, 400 sample trees with complete crown QSM reconstructions were retained for the final analysis (Fig. 5). The biomass was calculated by multiplying the QSM fitted cylinder volumes by wood density according to Eq. (1).

$$AGB_{PCD} = V_{QSM} * WD \quad (1)$$

where $AGB_{PCD}$ refers to biomass proxies from point clouds; $V_{QSM}$ is the volume of fitted cylinders; and $WD$ is the branch wood density from MacFarlane (2020). For simplicity, we assumed a uniform wood density throughout the tree crowns.

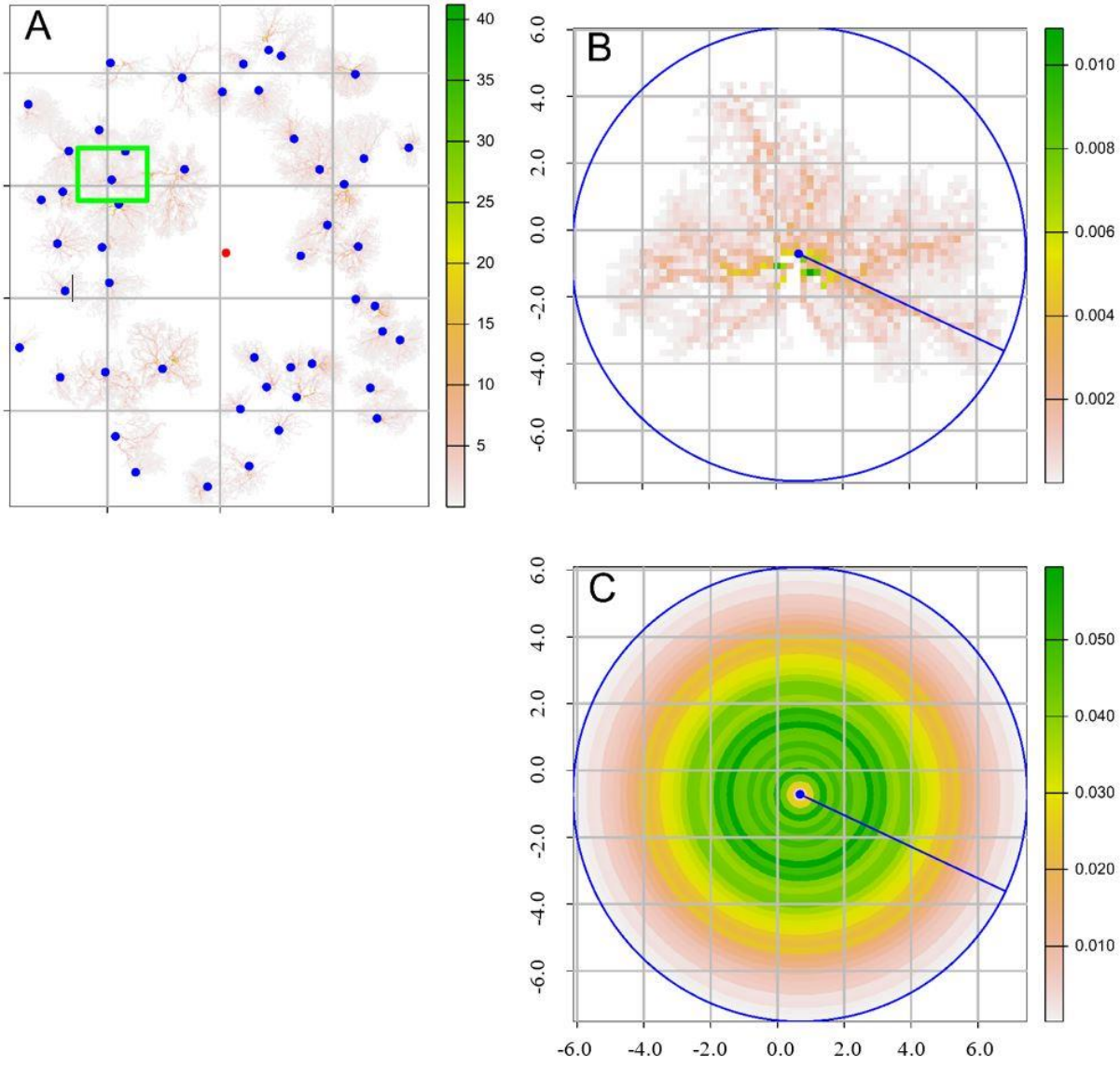


**Fig. 6.** Quantitative structure models (QSMs) of 74 final selected sample trees from one plot. The red colour represents the stems, and the dark grey colour denotes the crown parts.

### *2.3.2. Description of individual tree HBD*

To assign the spatial distribution of woody crown biomass, we first clustered the fitted cylinders into stems and crowns for individual trees using the QSM clustering algorithm (as illustrated in Fig. 6), following the definitions used by the Forest Global Earth Observatory (ForestGEO) (Arellano et al., 2021). The stem is considered to be the thickest, most upright, and longest woody component of the tree (red components in Fig. 6). The crown component was defined as the set of first-order branches originating from the stem and all other higher-order branches bifurcating from them (dark grey components in Fig. 6).

The crown biomass was computed from Eq. (1), and then projected horizontally (Fig. 7) for the empirical *HBD* model predictions as described in Section 2.3.4. We assigned the biomass distributions across the crown parts of individual trees based on 0.2 m spatial resolutions (Fig. 7B) or expressed in 0.2 m bin intervals along the distance from the stem (*DS*) (Fig. 7C), depending on the group of empirical models we employed (Section 2.3.4). The overall biomass along the *DS* is a function of the dimension and the angle of the branch components (fitted cylinders) from the vertical axis of the stem position. Here, we assumed that the horizontal projection area of the tree stem is very small (Fig. 6, Fig. 7); so in our *HBD* modelling, we focus on the crown biomass by disregarding the stem biomass.




277

278 **Fig. 7.** Process of describing crown biomass as a continuous horizontal distribution: (A) spatial
279 distribution of crown biomass (kg) over the whole plot; (B) the standardized spatial distribution of
280 crown biomass of a single tree (for the tree highlighted in the green box) at 0.2 m resolution; and (C)
281 aggregate of standardized crown biomass of the corresponding tree in 0.2 m circular bins around the
282 stem position (blue dot). The blue circle indicates the extent of the crown, assuming a circular crown
283 projection, and the blue line represents the distance from the stem (*DS*). See Table 2 for a description
284 of the variables.

285 *2.3.3. Variables for HBD models*

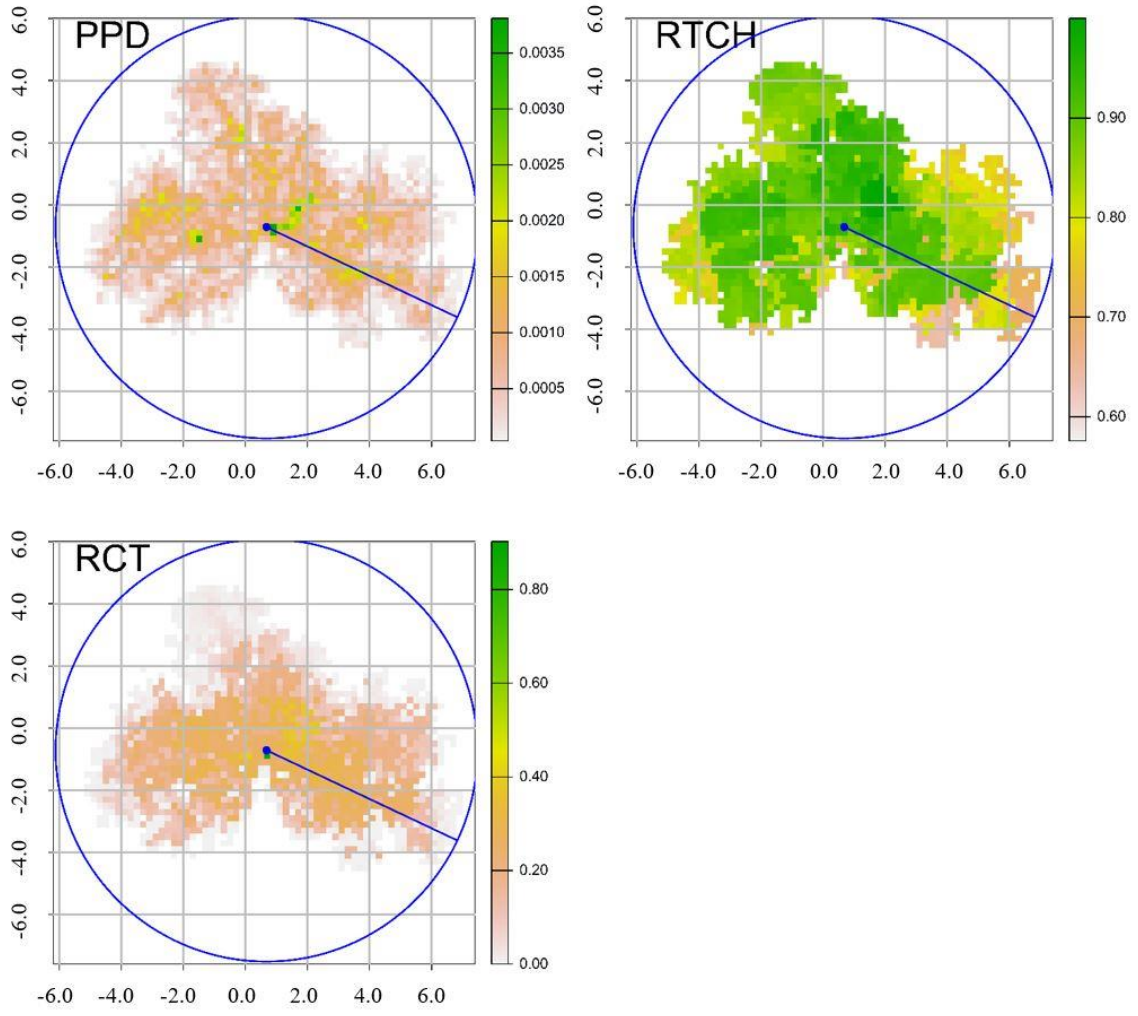
286 We considered various input tree and point cloud variables that could potentially improve the quality
287 of *HBD* models (Table 2). The description and computation of these variables are shown in Table 2.
288 The variables can be used in the empirical *HBD* modelling process depending on the applications in
289 forest inventory, and the need to describe crown biomass distributions that are close to the reality of
290 crown shape asymmetries and biomass variability of individual trees, as described in Section 2.3.4. The
291 relationships of the variables with the crown biomass distributions are shown in Fig. 9. The variables
292 that could significantly influence biomass distributions were identified by modelling a nonparametric
293 relationship of these variables, as presented in Fig. 9, with biomass distributions using multivariate
294 adaptive regression splines (Friedman, 1991). The selection process was based on generalized cross-
295 validation (GCV) criteria (Craven and Wahba, 1978) using the '*earth*' R package, version 5.3.4
296 (Milborrow, 2021). More details on the process of selecting the variables can be found in Appendix A.
297 Supplementary data (S1).

298 **Table 2.** Description and determination of tree and point cloud variables used to describe the *HBD*
299 models. The point clouds are based on the fusion of TLS and ULS datasets.

| Variable | Unit | Description | Origin | Measurement/ calculation/ reference |
|---|---|---|---|---|
| *H* | m | Tree height; the vertical distance between the base of the stem and the tree-top. | Point cloud | $Z_{max} - Z_{min}$ |
| *DBH* | cm | Diameter at breast height; the stem diameter at 1.3 m tree height. | Point cloud | Determined with circle-fitting approach of Terryn et al., 2023, implemented using *ITSMe* R package, version 1.0.0 (ITSMe, 2024). |
| *CL* | m | Crown length; the distance between the base of the lowest live branch and tree-top. | Point cloud | $Z_{max} - Z_{first\text{-}live\text{-}branch}$ |

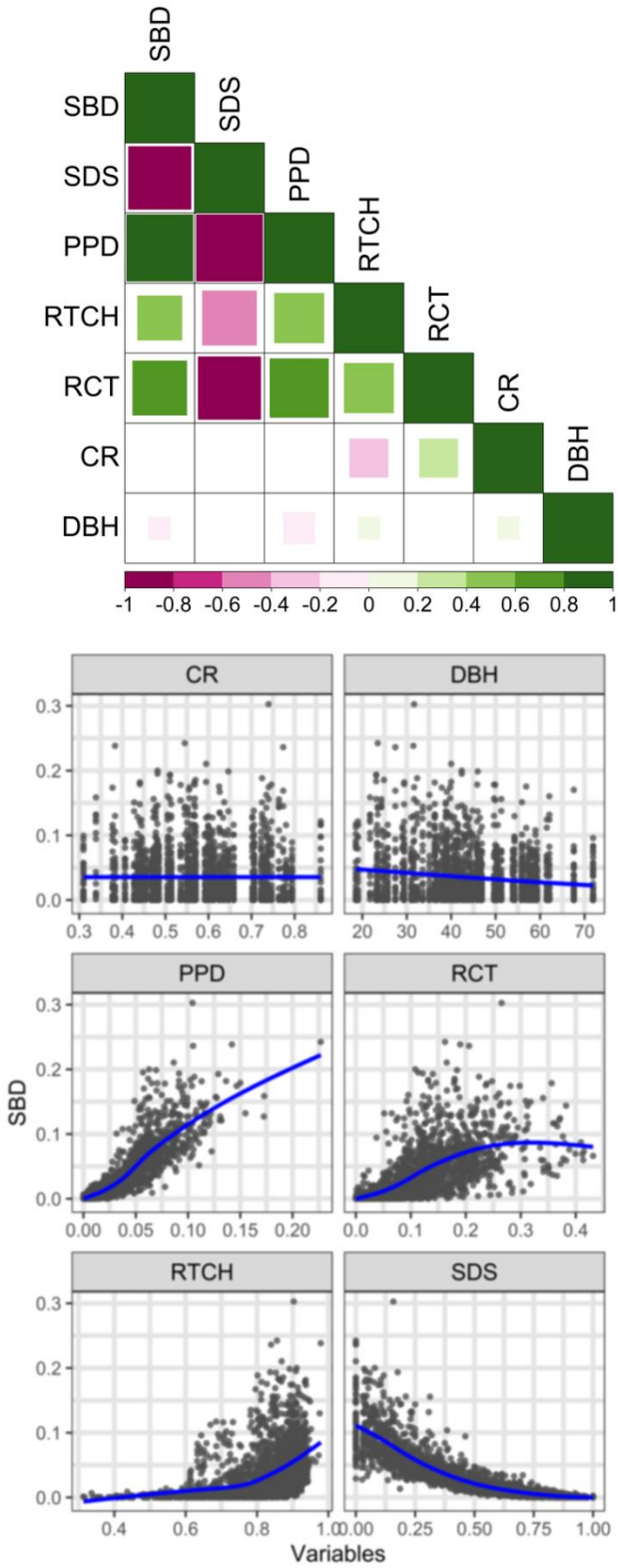
| | | | |
|---|---|---|---|
| *CR* | Crown ratio; the ratio of the crown length to the tree height. | Point cloud | *CL/H* |
| *SDS* | Standardized distance from the stem (i.e., crown diameter/2); the standardized horizontal distance along the stem position to the crown edge. | Point cloud | Horizontal distance to the stem (*DS*) was standardized on the scale [0 -1] (Fig. 8). Some groups of empirical horizontal biomass distribution (*HBD)* models have been described as a function of *DS* (Fig. 7, Section 2.3.4). |
| *PPD* | Point probability density; the LiDAR metrics that reflect the distribution of laser points across the entire crown of individual trees (Fig. 8). | Point cloud | The probability density of laser returns over the crown projection area of individual trees. For the empirical models, the probability density of laser returns per unit area (0.2 m pixel resolution) were extracted on the horizontal projection of tree crowns (Fig. 8). |
| *RTCH* | Relative top-of-crown height; the canopy height model across the crown parts of individual trees (Fig. 8). | Point cloud | Rasterization of the crown surfaces derived from the uppermost returns of the point clouds (i.e., CHM) (Lindberg et al., 2012). It was computed in 0.2 m pixel resolution across the crown projection area of individual trees, and standardized to the corresponding *H (top-of-crown height/H)* (Fig. 8). |
| *RCT* | Relative crown thickness; the crown thickness across the crown parts of the individual trees (Fig. 8). | Point cloud | Rasterization of the difference between the upper and the lower laser point returns at analogous positions (pixels) over the crown parts (Singh et al., 2015). It was computed in 0.2 m pixel resolution on the crown projection of individual trees, and |

| | | | |
|---|---|---|---|
| | | | standardized to the corresponding *H (crown thickness/H)* (Fig. 8). |
| *SBD* | Standardized biomass density; the standardized horizontal crown biomass distribution of individual trees around the stem axis along the horizontal *DS* or the specified pixel/ resolution. Empirical *HBD* models have been developed based on the *SBD* (Eq. (2)-Eq. (9)). | QSM, Empirical model | Crown biomass values were standardized to the *DS* scale [0-1] or in 0.2 m pixel across the crown projection area of trees. For the empirical *HBD* modelling in Eq. (4)-Eq. (9), the values per unit area (0.2 m pixel resolution) were extracted on the horizontal projection of the corresponding tree crowns (Fig. 7B), or extracted in 0.2 m bins along the radial direction (0-360°) around the stem axis (Fig. 7C) for the models in Eq. (2)-Eq. (3). |




300

**Fig. 8.** Model input variables (point probability density- *PPD*; relative top-of-crown height- *RTCH*; and relative crown thickness- *RCT*) of a single sample tree. The description and extraction processes are described in Table 2.



305 **Fig. 9.** Relationship between tree and point cloud variables vs. standardized biomass density (*SBD*).
306 *PPD*, *RTCH*, and *RCT* stand for point probability density, relative top-of-crown height, and relative
307 crown thickness, respectively. The variables are described in Table 2. The *SBD* was extracted as
308 described in Fig. 7. The upper plot shows the correlation matrix of these variables. The bottom plot
309 shows the scatterplots for *SBD* and the variables.

310 *2.3.4. Empirical models for HBD of individual trees*

311 The spatial distribution of crown biomass shown in Fig. 7 was empirically modelled using
312 segmented polynomial regression (Max and Burkhart, 1976), and a binary indicator (Farr, 2019)
313 functions. The modelling approach extends to the traditional taper curve models (Amna et al., 2020;
314 Cao, 2009; Salekin et al., 2021), and has also performed well to describe *HBDs* (Pérez-Cruzado et al.,
315 2021; Bazezew et al., 2024a).

316 The *HBD* models have been developed based on standardized values (standardized biomass density,
317 *SBD*) (Eq. (2)-Eq. (9)), as described in Table 2. The fitted models therefore do not provide absolute
318 biomass estimates but instead describe the relative biomass distribution across the crown projection
319 area of individual trees. For application to individual trees, total crown biomass must be derived from
320 other sources (e.g., proxies form laser-scanning datasets, or allometric models), after which the absolute
321 biomass can be distributed according to the identified *SBD* models (Eq. (2)-Eq. (9)).

322 We used multi-level *HBD* model fits (Eq. (2)-Eq. (9)) – some of the models (Eq. (2)-Eq. (3)) were
323 based on the description of biomass distributions assuming a circular crown projection area and
324 isotropic biomass distributions along the radial direction (0-360°) around the stem axis (as shown in
325 Fig. 7C), and other models (Eq. (4)-Eq. (9)) was used to potentially assign the biomass distributions
326 closer to the actual shape of the crowns, and also accounting for the associated biomass variability
327 within the crown parts of individual trees (as shown in Fig. 7B). The empirical modelling process is
328 provided in Appendix A. Supplementary data (S2).

329 Initially, we established empirical *HBD* models with a segmented polynomial regression function,
330 considering the biomass distribution as a function of *DS* and crown ratio (*CR*), formulated as in Eq. (2),

and Eq. (3). The empirical *HBD* prediction models in Eq. (2) and Eq. (3) were developed by considering simplifying theoretical assumptions (assuming perfectly upright stems, circular crown projection area of individual trees, and an isotropic biomass distribution around the stem axis).

$$SBD = b_1 * (SDS - 1) + b_2 * (SDS^2 - 1) + b_3 * (a_1 - SDS)^2 I_1 + b_4 * (a_2 - SDS)^2 I_2 + \varepsilon \quad (2)$$

where

$$\begin{cases} I_1 = 1, \text{if } SDS \leq a_1, \\ \quad = 0 \text{ otherwise;} \\ I_2 = 1, \text{if } SDS \leq a_2 \\ \quad = 0 \text{ otherwise.} \end{cases}$$

*SBD* denotes the standardized biomass density along the *DS*. The *SBD* can be modelled here by standardizing the biomass per unit area (average of 0.2 m pixel size) around the stem axis along the standardized distance from the stem (*SDS*), or based on the standardized cumulative or aggregate biomass in 0.2 m bins around the stem axis along the *SDS*. $b_1$-$b_4$ and $a_1$ and $a_2$ are the estimated model coefficients and inflection points, respectively; and $\varepsilon$ is the random error term. See Table 2 for details of variable descriptions and derivation methods.

An additional crown variable (crown ratio: *CR*) was integrated in Eq. (3). The coefficient $b_4$ in Eq. (2) was examined to be positively correlated with *CR* as a linear function [$b_4 = b_5$**CR*+$b_6$]. Accordingly, the biomass distribution was expressed as follows:

$$SBD = b_1 * (SDS - 1) + b_2 * (SDS^2 - 1) + b_3 * (a_1 - SDS)^2 I_1 + (b_5 * CR + b_6) * (a_2 - SDS)^2 I_2 + \varepsilon \quad (3)$$

where

$$\begin{cases} I_1 = 1, \text{if } SDS \leq a_1, \\ \quad = 0 \text{ otherwise;} \\ I_2 = 1, \text{if } SDS \leq a_2 \\ \quad = 0 \text{ otherwise.} \end{cases}$$

*SBD* and the modelling approach is as described in Eq. (2); $b_1$-$b_6$ and $a_1$ and $a_2$ are the model coefficients and inflection points to be estimated, respectively; and $\varepsilon$ is the random error term.

We have further developed various models to overcome the simplifying theoretical assumptions (Eq. (4)-Eq. (9)). Here, we incorporated additional crown and point cloud metrics (Table 2), where these variables were found to have quadratic relationships with biomass distributions as in Eq. (4)-Eq. (6) (overcome all the theoretical assumptions: perfectly upright stems, circular crown projection area of individual trees, and an isotropic biomass distribution), or by combining these variables with segmented polynomial regression and binary indicator functions as in Eq. (7)-Eq. (9) (overcome some of the theoretical assumptions: circular crown projection area of individual trees, and an isotropic biomass distribution).

$$SBD = b_5 * PPD^2 + b_6 * PPD + b_7 + \varepsilon \quad (4)$$

$$SBD = b_5 * RTCH^2 + b_6 * RTCH + b_7 + \varepsilon \quad (5)$$

$$SBD = b_5 * RCT^2 + b_6 * RCT + b_7 + \varepsilon \quad (6)$$

where *SBD* denotes as described in Eq. (2). *PPD*, *RTCH*, and *RCT* stand for point probability density, relative top-of-crown height, and relative crown thickness of individual trees (in 0.2 pixel resolutions), respectively (see Table 2 and Fig. 8). The values have been extracted at the corresponding cells across the crown projection area of individual trees where *SBD* is to be predicted. $b_5$-$b_7$ are the estimated model coefficients; and ε is the random error term.

In the models of Eq. (7)-Eq. (9), the segmented polynomial regression model of Eq. (2) and the quadratic functions of Eq. (4)-Eq. (6) have been combined for describing biomass variabilities across the crown parts of individual trees, along with the integration of the binary functions to account for crown shape asymmetries and biomass variabilities. The *HBD* models were formulated as follows:

$$SBD = (b_1 * (SDS - 1) + b_2 * (SDS^2 - 1) + b_3 * (a_1 - SDS)^2 I_1 + b_4 * (a_2 - SDS)^2 I_2) + (b_5 * PPD^2 + b_6 * PPD + b_7)) * \max(0, PPD! = 0) + \varepsilon \quad (7)$$

$$SBD = (b_1 * (SDS - 1) + b_2 * (SDS^2 - 1) + b_3 * (a_1 - SDS)^2 I_1 + b_4 * (a_2 - SDS)^2 I_2) + (b_5 * RTCH^2 + b_6 * RTCH + b_7)) * \max(0, RTCH! = 0) + \varepsilon \quad (8)$$

$$SBD = (b_1 * (SDS - 1) + b_2 * (SDS^2 - 1) + b_3 * (a_1 - SDS)^2 I_1 + b_4 * (a_2 - SDS)^2 I_2) + (b_5 * RCT^2 + b_6 * RCT + b_7)) * \max(0, RCT! = 0) + \varepsilon \quad (9)$$

where in Eq. (7)-Eq. (9):

$$\begin{cases} I_1 = 1, \text{if } SDS \leq a_1, \\ \quad = 0 \text{ otherwise;} \\ I_2 = 1, \text{if } SDS \leq a_2 \\ \quad = 0 \text{ otherwise.} \end{cases}$$

$$\begin{cases} \max(0, PPD! = 0) = 1, \text{if } PPD \neq 0, \\ \qquad\qquad = 0 \text{ otherwise;} \\ \max(0, RTCH! = 0) = 1, \text{if } RTCH \neq 0, \\ \qquad\qquad = 0 \text{ otherwise;} \\ \max(0, RCT! = 0) = 1, \text{if } RCT \neq 0; \\ \qquad\qquad = 0 \text{ otherwise.} \end{cases}$$

*SBD* denotes as described in Eq. (2). *PPD*, *RTCH*, and *RCT* as described in Eq. (4)-Eq. (6); $b_1$–$b_7$, and $a_1$ and $a_2$ are the model coefficients and inflection points, respectively; and $\varepsilon$ is the random error term. The '*max(0,PPD!=0)*'; '*max(0,RTCH!=0)*'; and '*max(0,RCT!=0)*' denote the binary indicator functions. This means that the values of the corresponding variables are assigned as *'TRUE'* or *'1'* if within the crown projection extents, otherwise assigned as *'FALSE'* or *'0'* on empty spaces or pixels (Fig. 8) – representing the actual shape of the tree crowns.

### *2.3.5. Model validation and statistical analysis*

Crown biomass spatial distributions (Fig. 7) and empirical *HBD* model predictive variables (Table 2, Fig. 8) were derived from point clouds. For these variables, there was no "true" reference data from observations in the field, so we relied on the fusion laser point datasets as our benchmark or reference. Deriving such variables in the field or with direct measurements, especially in forest stands, may demand additional effort, and such measurements cannot always be assumed to be unbiased. In

particular, for describing biomass distribution (Fig. 7) in structurally complex crowns and larger trees, direct measurements are hardly feasible and, if done, may also carry substantial uncertainties. This is because, projecting crown biomass onto a horizontal plane would require quantifying biomass across multiple cross-sections of each branch order and determining the angles of each section – that is impossible using field methods. Therefore, the use of field methods would be neither convenient for describing *HBD* nor applicable for validating the point cloud-based *HBD* models. Alternatively, point clouds offered additional advantages, resulting in a quite complete 3D structure of the trees (Fig. 3, Fig. 4, Fig. 6), which can allow reliable derivation of crown variables (Table 2, Fig. 8) and description of spatial crown biomass distributions (Fig. 7) more conveniently and efficiently than field measurements. Furthermore, the fused TLS and ULS point clouds (Fig. 3) do offer a solution to increase the robustness and accuracy of extracting crown attributes in complex forest stands, and can thus be used as a reference for developing and validating models.

The suitability of the empirical *HBD* models in predicting biomass distributions across the crown projection area of individual trees was assessed by cross-validation using various statistical performance measures (Eq. (10)). For the cross-validation, the full datasets of 400 fully crown reconstructed sample trees was randomly partitioned using simple random sampling – specifically, 320 trees (80%) were randomly selected for model calibrations, and the remaining 80 trees (20%) were used to form the validation datasets. The random selection was performed in R using the *sample ()* function (R Core Team, 2024). We reported the established statistical measures for established models, such as root mean square error (*RMSE*), relative mean square error (*reRMSE*), bias, and relative bias (*reBias*) (Eq. (10)). Further, we used the concordance correlation coefficient (*CCC*) (Lin, 1989) to evaluate the agreement between the *HBD* model estimates and the corresponding reference biomass distributions (Eq. (10)). The *CCC* measures the agreement between modelling approaches by quantifying the distance from the 1:1 line. *CCC* values range from -1 (perfect disagreement) to 1 (perfect agreement), and 0 is no agreement.

$$\begin{cases} RMSE = \sqrt{\frac{1}{n}\sum_{i=1}^{n}(HBD_{model} - HBD_{ref})^2} \\ reRMSE = \frac{RMSE}{mHBD_{ref}} * 100\% \\ Bias = \frac{1}{n}\sum_{i=1}^{n}(HBD_{model} - HBD_{ref}) \\ reBias = \frac{Bias}{mHBD_{ref}} * 100\% \\ CCC = \frac{2\rho\sigma_{12}}{\sigma^2{}_{HBD_{ref}} + \sigma^2{}_{HBD_{model}} + (mHBD_{ref} - mHBD_{model})^2} \end{cases} \quad (10)$$

where $HBD_{model}$ represents the empirical *HBD* model estimates at any direction and for a given area of the crown projection along the *DS*; $HBD_{ref}$ is the corresponding reference biomass (biomass distributions from point cloud derivations); $mHBD_{model}$ is the mean *HBD* model estimates; $mHBD_{ref}$ is the mean *HBD* of the reference values; $\rho$ is the correlation coefficient of the two estimates; $\sigma_{12}$ is the covariance of the reference and empirical *HBD* model estimates; $\sigma^2$ is the variances of the reference values and model estimates; and $n$ is the number of observations.

## 3. Results

Empirical *HBD* models describing crown biomass distributions as a function of horizontal distance from stem (*SDS*) were developed from the proposed functions in Eq. (2)-Eq. (9). The estimated coefficients, along with the corresponding model assumptions are presented in Table 3. The models have been developed based on the standardized biomass density (*SBD*) predictions at the 0.2 m pixel resolution level as described in Fig. 7B and in Eq. (4)-Eq. (9), or based on the aggregate crown biomass distributions in 0.2 m bins around the stem axis in the radial directions, as shown in Fig. 7C, (Eq. (2) and Eq. (3). For the models of Eq. (2) and Eq. (3), the biomass density can be described empirically, and the corresponding model fits are shown in Fig. 10. For such empirical *HBD* models, the biomass distribution showed a higher variability of biomass density close to the stem (*SDS* ≈ 0-0.4) and became more consistent around the crown edges (Fig. 10).

When comparing the models, Eq. (2) and Eq. (3) offered *HBD* predictions by assuming a perfectly upright stem, circular crown projection area, and isotropic biomass distributions, as shown in Fig. 7C. Conversely, the models established based on Eq. (4)-Eq. (9) provided *HBD* distributions by accounting for crown shape asymmetries and associated biomass variabilities, as in Fig. 7B. Accordingly, the models by Eq. (4)-Eq. (9) assigned biomass distributions within the real crown shape extents and with biomass variabilities across the crown projection area of individual trees. Since these models are based on the actual crown geometry of individual trees (see Fig. 7B), the biomass distributions are described only in a spatially explicit manner across the crown projection areas. The model developments and validations have therefore been performed through biomass cross-matching at the pixel levels with reference biomass distributions. The corresponding performance of the models is shown in Fig. 11, and Table 4.

**Table 3.** Estimated coefficients and model assumptions for the horizontal biomass distribution (*HBD*) models (Eq. (2)-Eq. (9)), and the corresponding model fit standard errors (*SE*) at the 95% confidence level of significance. The *HBD* is modelled based on the standardized biomass density (*SBD*), which is expressed as the probability of the biomass density along the horizontal distance from the stem (*DS*) at a pixel size of 0.2 m over the crown projection area of the individual trees (as shown in Fig. 7B). The *HBD* models of Eq. (2) and Eq. (3) (Fig. 7C) were presented based on the average *SBD* in a 0.2 m pixel size around the stem axis along the *DS* scale [0-1] or based on the cumulative or aggregate *SBD* in 0.2 m bins around the stem axis on the *DS* scale [0-1]. See Fig. 10 for the corresponding model fits of Eq. (2) and Eq. (3), which can be empirically described as a function of *DS*.

| | Coefficients and model-fit statistics [biomass at a 0.2 m pixel; biomass aggregates in 0.2 m bins around the stem axis along *DS*] | | | | | | | | | | | Model assumptions | | |
|---|---|---|---|---|---|---|---|---|---|---|---|---|---|---|
| Model | $b_1$ | $b_2$ | $b_3$ | $b_4$ | $b_5$ | $b_6$ | $b_7$ | $a_1$ | $a_2$ | *SE* | *P-value* | Circular crown projection area | Isotropic biomass distribution | Perfectly upright stem |
| Eq. (2) | [-0.0014; -0.1622] | [-0.0001; 0.0801] | [-0.0184; -1.1675] | [0.004; 0.137] | | | | [0.11; 0.11] | [0.45; 0.54] | [0.0332; 0.0335] | [7.72E-63; 7.79E-63] | + | + | + |
| Eq. (3) | [0.0001; -0.1588] | [-0.0010; 0.0781] | [-0.0149; -1.1744] | | [0.0042; 0.0928] | [0.001; 0.083] | | [0.09; 0.11] | [0.62; 0.55] | [0.0371; 0.0380] | [1.44E-48; 1.46E-48] | + | + | + |
| Eq. (4) | | | | | -3.2E+01 | 1.749 | 0.0001 | | | 0.0239 | 2.43E-84 | – | – | – |
| Eq. (5) | | | | | 0.0077 | -0.008 | 0.0024 | | | 0.0276 | 4.808E-52 | – | – | – |

| | | | | | | | | | | | | | | |
|---|---|---|---|---|---|---|---|---|---|---|---|---|---|---|
| Eq. (6) | | | | | -0.0089 | 0.009 | 0.0001 | | | 0.0328 | 7.724E-63 | – | – | – |
| Eq. (7) | 0.0001 | -0.0007 | 0.0009 | 0.0018 | 5.E+02 | 0.361 | 0.0000 | 0.61 | 0.49 | 0.0251 | 4.573E-72 | – | – | + |
| Eq. (8) | -0.002 | 0.0004 | -0.0222 | 0.0056 | 0.0010 | -0.001 | 0.0004 | 0.12 | 0.35 | 0.0305 | 4.432E-50 | – | – | + |
| Eq. (9) | -0.0034 | 0.0010 | -0.0018 | 0.0032 | 0.0073 | -0.001 | 0.0000 | 0.85 | 0.53 | 0.0252 | 3.244E-56 | – | – | + |

+ Consider the corresponding assumptions; – Do not consider the assumptions.

441

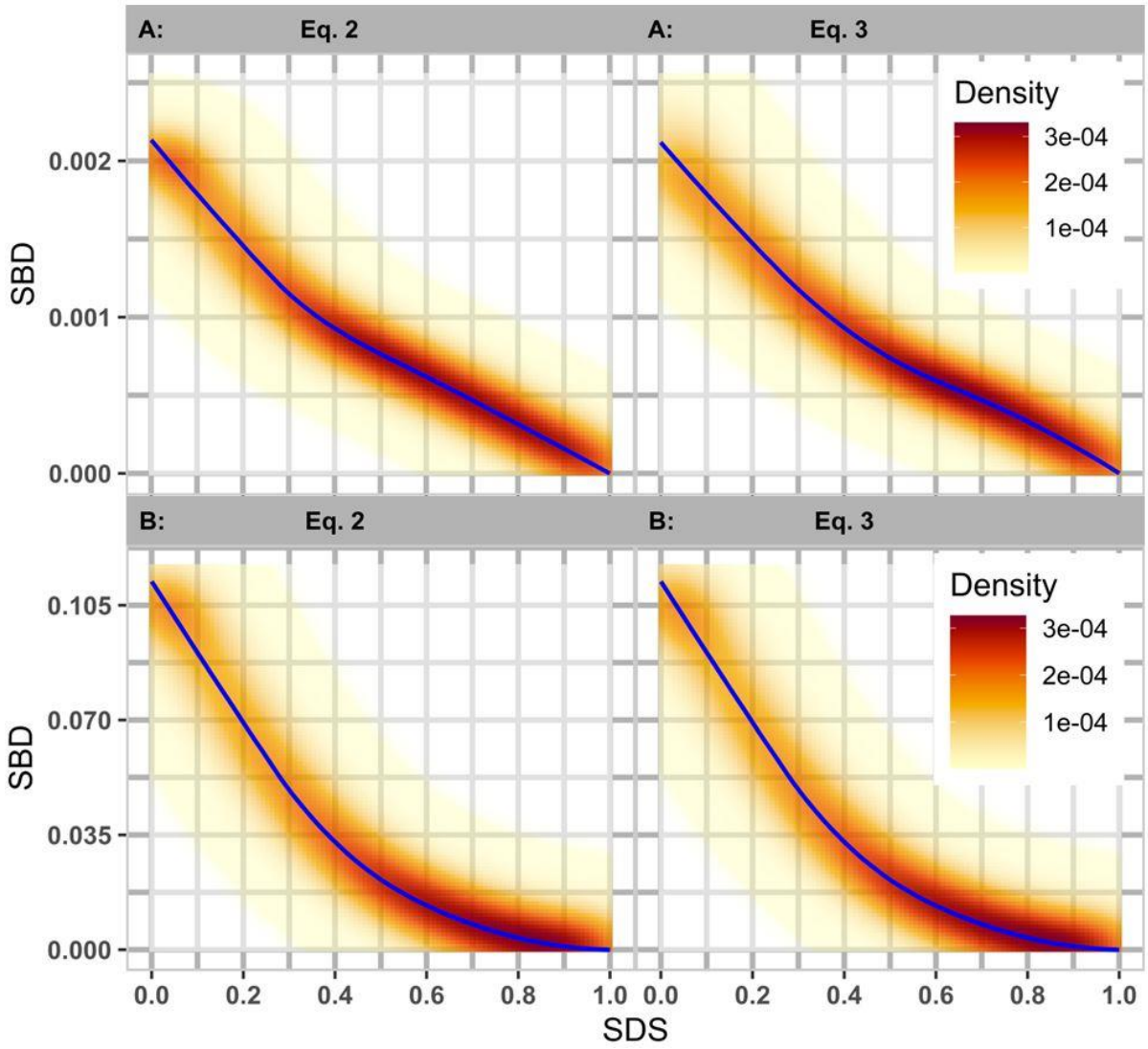
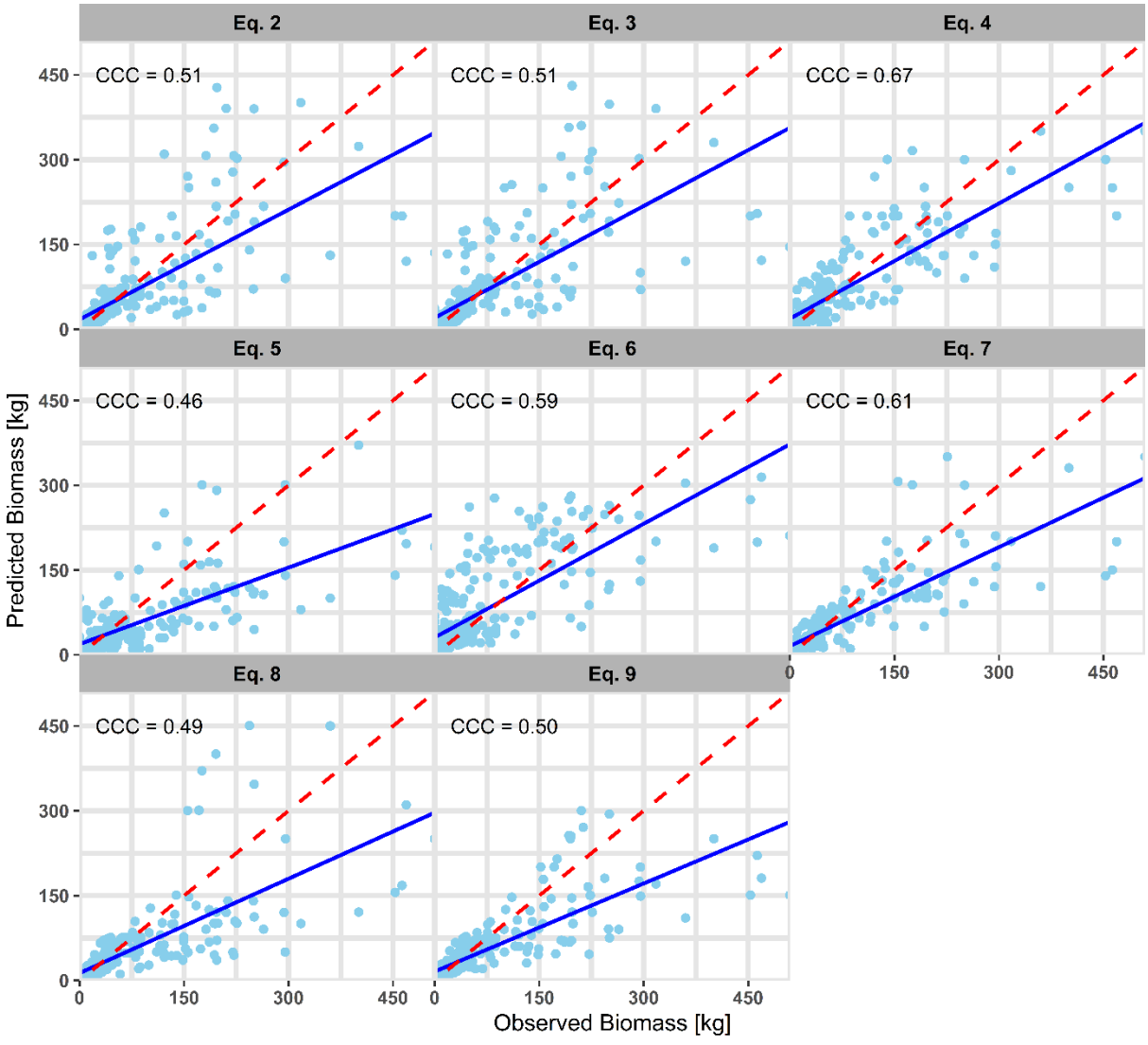



**Fig. 10.** Empirical *HBD* prediction nonparametric regression fitted lines developed from the models in Eq. (2) and Eq. (3). Eq. (4)-Eq. (9) are described only in a spatially explicit manner across the crown projection area of individual trees. A: Standardized biomass density (*SBD*) described as an average of 0.2 m pixel level around the stem axis along the standardized distance from the stem (*SDS*). B: Corresponding *HBD* models expressed as a cumulative or aggregate of *SBD* in 0.2 m bins around the stem axis along the *SDS*. The estimated parameters of the corresponding distribution models are shown in Table 3. The density (probability) colour palette represents the distribution of data point fits.

The performance of the *HBD* models (Eq. (2)-Eq. (9)) was evaluated by comparing the model *HBD* estimates with the reference spatial distribution of crown biomass derived from the QSM proxies (Fig. 11, Table 4). It was done by comparing biomass distributions in analogous areas at any crown parts

along the distance from the stem position of the corresponding trees (see Fig. 12). This was a measure of how well the total crown biomass was distributed over the crown projection area of the respective trees. The highest level of model performance refers to the crown biomass being determined for each section of the crown projection area of the corresponding trees as accurately as possible, i.e., the total crown biomass was distributed or assigned well close to the actual crown shapes, and on the basis of the associated biomass variability. The models had coefficients of determination ($R^2$) ranging from 0.49-0.70 (Fig. 11); with the highest $R^2$ for Eq. (4). The model in Eq. (4) showed a better performance in describing *HBDs* with a *CCC* of 0.67 (Fig. 11) and an error of ≈27 kg (44%) (Table 4). The models in Eq. (2) and Eq. (3) resulted in higher errors of ≈45 kg (58%) (Table 4), with the model performance depending mainly on the stem irregularity, structure and shape of the tree crowns.



464 **Fig. 11.** Comparison of empirical horizontal biomass distribution (*HBD*) model predictions (Eq. (2)-
465 Eq. (9)) with reference to spatial crown biomass distributions. The blue line indicates the model fit. The
466 dashed red line denotes the 1:1 line along with the corresponding *CCC*. A summary of the model
467 performance measures is presented in Table 4.

468 **Table 4.** Summary of the performance of horizontal biomass distribution (*HBD*) models (shown in
469 Table 3) when validated against reference biomass distributions.

| | Performance measure | | |
|---|---|---|---|
| Model | $R^2$ | *RMSE* (kg; %) | *Bias* (kg; %) |
| Eq. (2) | 0.49 | 45.42; 58.54 | -6.06; -10.44 |
| Eq. (3) | 0.49 | 45.08; 58.21 | -5.95; -8.22 |
| Eq. (4) | 0.70 | 27.37; 43.66 | -2.23; -5.94 |
| Eq. (5) | 0.54 | 34.28; 54.68 | -12.42; -22.61 |
| Eq. (6) | 0.56 | 29.94; 47.77 | 10.20; 19.28 |
| Eq. (7) | 0.64 | 37.43; 59.72 | -12.67; -23.02 |
| Eq. (8) | 0.53 | 40.63; 64.82 | -14.87; -23.74 |
| Eq. (9) | 0.60 | 43.42; 69.36 | -14.35; -22.90 |

470 ## 4. Discussion

471 Given the complex structure of tree crowns, simulating realistic *HBD* models is also complex, and
472 the modelling approaches should consider applications in forest inventories. Accordingly, three ways
473 of *HBD* modelling have been proposed in this study. The first set of models in Eq. (2) and Eq. (3) (Table
474 3) were developed under simplifying modelling assumptions: the perfectly upright stem, the circular
475 crown projection area of trees, and the isotropy of biomass distributions (Fig. 7C, Fig. 12). By these
476 assumptions, stem irregularities, crown shape asymmetries and the associated variability in biomass
477 distribution across crown parts were disregarded. The biomass distribution models were developed
478 based on either standardization of biomass distributions per unit area around the stem axis along the
479 standardized horizontal distance from the stem (*SDS*) (Fig. 10A) or standardized aggregate biomass

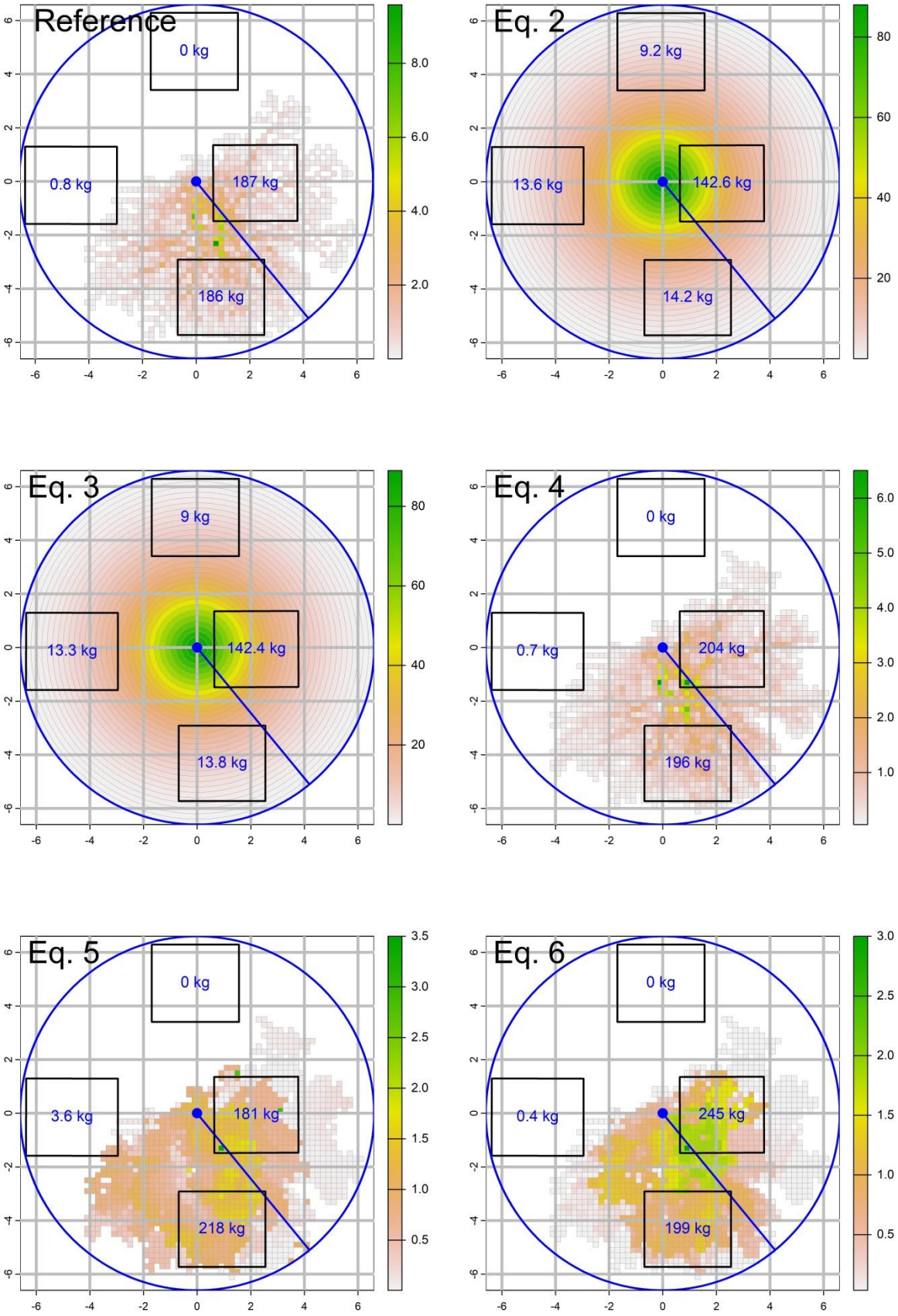
around the stem along the *SDS* (Fig. 10B). Previous studies on *HBD* (Bazezew et al., 2024a; Kleinn et al., 2020; Pérez-Cruzado et al., 2021) have also employed similar assumptions. Mascaro et al. (2011) described crown biomass distribution by considering an identical biomass density across the entire crown projection area of individual trees, i.e., a uniform horizontal biomass distribution. The second set of *HBD* models, in particular Eq. (4)-Eq. (6) (Table 3), are considering a more realistic structure of tree crowns: the models were parameterized with additional crown and point cloud metrics (Table 2, Fig. 8), which allow the description of *HBDs* by accounting for stem irregularities, crown shape asymmetries and biomass variability. These models allow depicting the *HBDs*, as shown in Fig. 7B and Fig. 12. The third group of models (Eq. (7)-Eq. (9)) (Table 3) have also been developed by accounting for crown shape asymmetries and biomass variability. These models have considered the assumption of a perfectly upright stem for individual trees.

Crown biomass distributions were variable, predominantly closer to the stem (*SDS* ≈ 0-0.4), where most of the crown biomass portions occur (Fig. 10). The variability of biomass density decreases towards the crown edges, which is near the vicinity of crown parts with finer branches (Fig. 10, Fig. 12). The variability is mostly due to complex crown structures, such as varying branch angles both between and within branch orders. Larger trees typically have multiple trunks with irregular stems. In such cases, the tree stems are not perfectly vertical or are rarely oriented at a 90◦ vertical angle. Variability in crown shape is certainly a source of variation in the prediction of biomass distributions, and this is mainly the case for the models in Eq. (2) and Eq. (3). Further, biomass distribution models may be slightly influenced by variations in point cloud density, particularly in complex crown structures and plots with high occlusions, such as plots with dense and high understory vegetation. We avoided scanning in rainy conditions, which has a risk of laser pulse transmission and scattering (Wilkes et al., 2017). However, slightly windy conditions might have affected the quality of the point clouds at some scan positions, which was hardly to avoid if it occurred after the scans had started. Scanning under windy conditions (>5 $m.s^{-1}$) moves trees and affects biomass allocation (Dassot et al., 2011). Such wind-related problems are particularly pronounced in the upper parts of the canopy (Vaaja et al., 2016), and thus may also influence laser scanning-based biomass proxies (Fig. 6).

Consideration of various model assumptions may influence the level of uncertainty in biomass distributions and approaches in forest inventory applications. The first assumption made by considering the stems to be perfectly upright in Eq. (2) and Eq. (3), and Eq. (7)-Eq. (9) may not always be the case, particularly for larger trees with multiple trunks. This can lead to uncertainties, principally for biomass densities closer to the stem as demonstrated in Fig. 12. Second, for some of the models (Eq. (2) and Eq. (3)), the assumption of a circular crown projection area of individual trees disregards the ever-present crown shape asymmetries. This may also introduce considerable errors (Table 4), with the level of uncertainty depending on the dimension and complexity of the crown structures. For example, a sample of individual tree biomass distributions illustrating this is shown in Fig. 12; where the actual crown projection area is 57 $m^2$, but becomes more than double (≈136 $m^2$) if a circular projection area is assumed. In this case, ≈220 kg of the total crown biomass (902 kg) was assigned by these models to the area not within the actual crown projection areas. Lastly, also in the case of Eq. (2) and Eq. (3), the assumption of isotropic biomass distributions around the stem axis is unlikely to be the case in particular for large trees. As illustrated in Fig. 12 (reference distributions), in most cases, the biomass distribution varies considerably across the crown parts of individual trees. In general, all of these model assumptions may be essential to simplify the empirical modelling approaches, but it should be noted that they carry, of course, uncertainties. The main advantage of such simplified models is that once developed with a sufficiently large sample of trees, their application may better be generalized without the need for individual laser scans. Although these models ((Eq. (2), Eq. (3), Eq. (7)-Eq. (9)) exhibit larger errors in our current forest scans, as shown in (Table 4), they may still be reasonably well suited for describing biomass distributions in forests dominated by relatively small-dimension trees with regular stems and single trunks.

Models established by incorporating crown and point cloud metrics (Eq. (4)-Eq. (9)) (Table 3) can assign crown biomass distributions in the area defined by the exact crown projection extents and with corresponding crown biomass variability of individual trees (Fig. 12). The model in Eq. (4), developed by linking the probability of point density (*PPD*) and by accounting for the crown shape asymmetries, stem irregularities, and biomass variabilities, provides a good proxy for the biomass distributions (Fig.

11, Table 4). However, it should be noted that the model performance may depend on the quality of the point clouds, which can be affected by the complexity of the forest structure, tree dimensions and the laser devices (Abegg et al., 2023; Dassot et al., 2011; Griebel et al., 2015; Li et al., 2020; Singh et al., 2015; Morhart et al. 2024). The *PPD*-based *HBD* predictions may therefore be a robust function in leaf-off scans where there are sufficient laser penetrations in the inner parts of the crowns. In our study, which uses fused TLS and ULS datasets under leaf-off conditions (Section 2.2), and with further rigorous selection of sample trees with complete crown reconstructions (Section 2.3.1), the point-cloud quality is sufficiently good and is unlikely to have a significant influence on the developed models. Alternatively, models that include additional inputs, such as the canopy height model (Eq. (5), Eq. (8)) and crown thickness (Eq. (6), Eq. (9)) (Table 3), may be used when applied in leaf-on scans or with dense crown structures, as these metrics are calculated only from laser reflections of crown surfaces.


Reference
0 kg
0.8 kg
187 kg
186 kg
Eq. 2
9.2 kg
13.6 kg
142.6 kg
14.2 kg
Eq. 3
9 kg
13.3 kg
142.4 kg
13.8 kg
Eq. 4
0 kg
0.7 kg
204 kg
196 kg
Eq. 5
0 kg
3.6 kg
181 kg
218 kg
Eq. 6
0 kg
0.4 kg
245 kg
199 kg

545

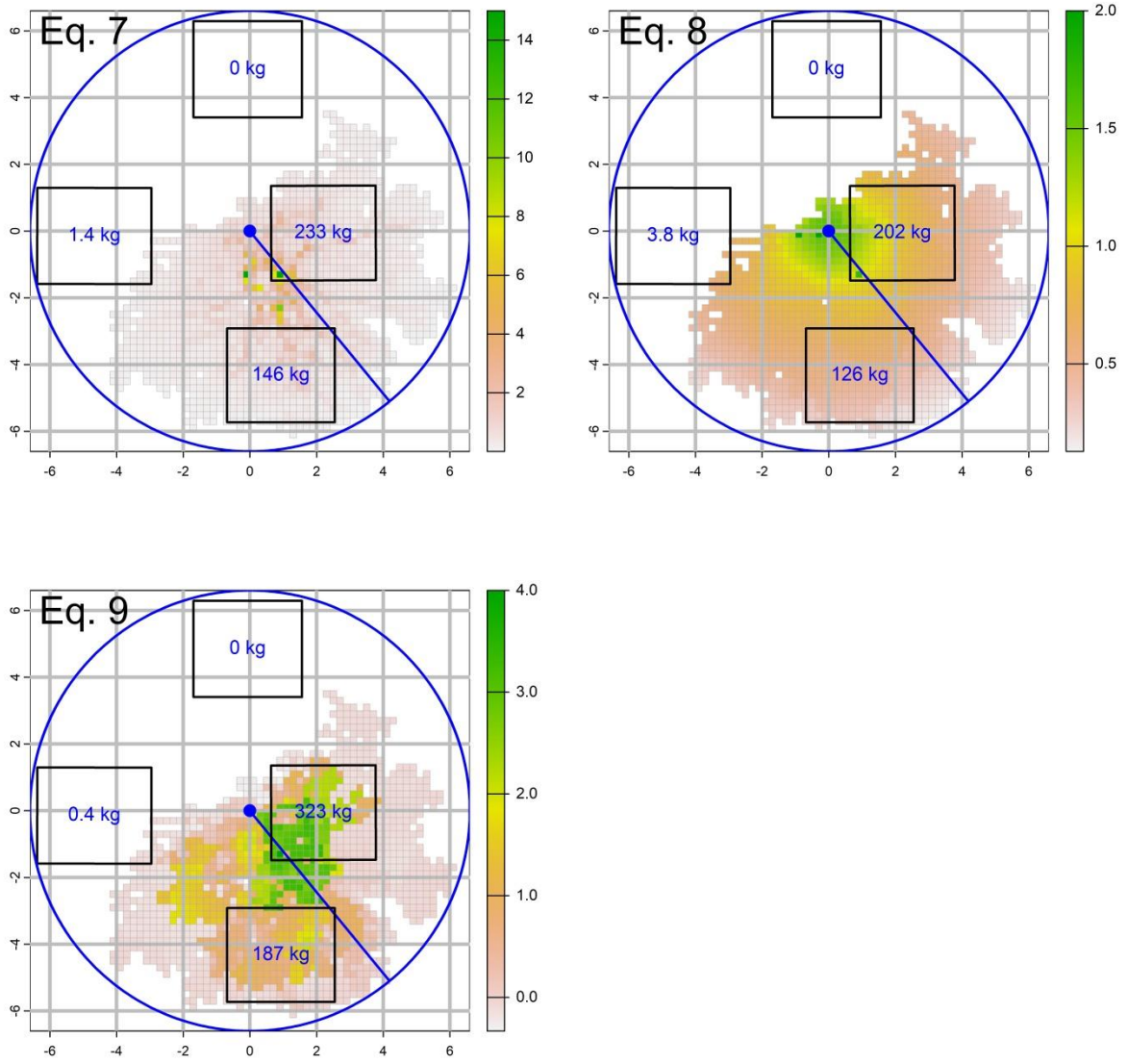



**Fig. 12.** Horizontal biomass distributions (*HBDs*) of a single sample tree, depicted with various models (Eq. (2)-Eq. (9)). The total tree crown biomass is 902 kg. The (reference) biomass distribution is based on the proxy from the QSM cylinder-fits. The aggregate biomass within the sample of square boundaries (≈10 $m^2$ each) shown at various random locations illustrates the variability and comparison of biomass distributions across the empirical *HBD* models in use. The actual crown projection area is 57 $m^2$, while assuming a circular crown projection extent (the blue circle) becomes 136 $m^2$. The blue dot denotes the stem position, and the blue line represents the distance from the stem position (*DS*).

In this study, the models were developed and validated using the point cloud datasets. This approach is found to be suitable and convenient for describing *HBDs*, which are otherwise impractical with field

556 or direct measurements. Doing direct measurements of crown variables in the field, especially in forest
557 stands, would be extremely difficult and expensive - if not impossible. In particular, for describing the
558 spatial biomass distributions (Fig. 7) and crown metrics (Fig. 8) in complex crowns and larger trees,
559 direct measurements are hardly feasible and, if done, would carry substantial uncertainties. In addition,
560 direct measurements are necessarily destructive and thus may not be possible in many situations, such
561 as in protected areas, parks and urban forests (Liang et al., 2014). Alternatively, estimations and
562 measurements of tree crown metrics from laser scanning offer results that may even be more accurate
563 than field methods (Bazezew et al., 2018; Ojoatre et al., 2019; Qi et al., 2022; Srinivasan et al., 2015).
564 The point clouds resulting from the fusion of the TLS and ULS datasets provide improved point cloud
565 densities over large portions of the crowns of individual trees (Fig. 3), and thus can offer reliable crown
566 biomass estimates (Fig. 6) and crown variables (Table 2, Fig. 8). A TLS scan layout with elevated-
567 tripod scans (Section 2.1) is an additional advantage that can also significantly reduce occlusion effects,
568 as reported by Griese et al. (2025), and thus may improved the crown biomass proxies and description
569 of *HBDs* (Fig. 7).

570 Laser points from leaf-off conditions increase laser penetration through the forest canopy. This
571 reduces the errors in QSM branch reconstructions and diameter estimates (Calders et al., 2015; Momo
572 Takoudjou et al., 2018; Raumonen et al., 2013; Terryn et al., 2023). However, scanning in the leaf-off
573 period disregards foliage biomass because QSM can only reconstruct the woody parts of the crown.
574 Estimating foliage biomass distributions using point clouds may lead to higher uncertainties due to
575 occlusion effects (Lau et al., 2019). The proportion of (the seasonal) leaf biomass in deciduous trees is
576 likely to be relatively low when compared to the (permanent) woody biomass (Daryaei and Sohrabi,
577 2016). When required, empirical models derived from direct measurements (Kershaw and Maguire,
578 1996; Xu and Harrington, 1998) can be a convenient way to describe the spatial distribution of foliage
579 biomass. It should also be noted that our approach may not be directly applicable to conifer species; in
580 particular, QSM reconstructions under coniferous crown structures are often challenging and associated
581 with high uncertainties (Raumonen et al., 2013). Thus, alternative approaches may be required for
582 retrieving crown biomass for coniferous tree species.

## 5. Conclusions

The following conclusions can be drawn from this research:

- The *HBD* was empirically modelled with a frequently used taper curve model and integration of binary indicator functions, with the fitting models showing comparable shapes to the common stem taper curves.
- We proposed alternative empirical *HBD* models, which can offer the closest reality of crown biomass distributions by accounting for the ubiquitous crown shape asymmetries and associated biomass variabilities of individual tree crowns. Some models have also been developed assuming perfectly upright stems, circular crown projection areas and isotropy of biomass distributions, which may be chosen depending on the availability of laser devices and practical applications in forest field inventory.
- We derived crown and point cloud metrics from the fusion of TLS and ULS datasets, and the methodologies employed to describe the spatial distribution of crown biomass from laser points are convenient and efficient ways that may otherwise be impractical with direct measurements. Fusion of TLS and ULS point clouds may be essential for highly accurate reference biomass distributions and thus for the development of reliable *HBD* models. Once realistic approximations of *HBD* functions are available for use in forest inventories, they can also be applied to aboveground biomass values derived from allometric models.
- Our *HBD* approach is expected to improve the accuracy of remotely sensed forest biomass models, as the plot biomass aggregates from *HBDs* are more closely registered to remote sensing metrics, as demonstrated in Kleinn et al. (2020). Here, tree-level biomass maps are spatially aggregated within fixed-area plots or across inventory grids, ensuring that only the portions of biomass vertically intersecting each sampling unit are included. When combined with high-resolution remote sensing datasets, such as airborne LiDAR, UAV imageries, or satellite-based canopy metrics, the *HBD*-derived plot biomass aggregates can enable more precise spatial matching between field observations and remotely sensed signals. This co-registration may minimize the biases caused by crown overlaps over the fixed-plot boundaries,

which are common in conventional-based biomass estimation approaches. Integrating *HBD* into forest monitoring thus expected to enhance the calibration of remote sensing biomass models, supports consistent biomass accounting across varying plot geometries and sizes. Further, *HBD* approach may facilitates spatially explicit analyses of canopy fuel distributions, and modelling of the proportion of biomass losses in crown disturbance effects.

## Funding

The first author is supported by the German Academic Exchange Service (DAAD) with a research grant for Doctoral Programmes in Germany (number: 57507871). Nils Griese is funded by the Deutsche Forschungsgemeinschaft (DFG, German Research Foundation) in the project number: 496533645.

## Declaration of competing interest

The authors declare that they have no known competing financial interests or personal relationships that could have appeared to influence the work reported in this paper.

## Data availability

Data will be made available upon request.

## Acknowledgments

We acknowledge the German Academic Exchange Service (DAAD) (Germany) for funding, and the Georg-August-Universität Göttingen (Germany) and Debre Berhan University (Ethiopia) for supporting with data collection and computational resources. The authors also thank the editor and anonymous reviewers for their valuable comments.

## Appendix A. Supplementary data

Supplementary material to this article can be found online at ----------.

## References


Abegg, M., Bösch, R., Kükenbrink, D., & Morsdorf, F. (2023). Tree volume estimation with terrestrial laser scanning — Testing for bias in a 3D virtual environment. *Agricultural and Forest Meteorology*, *331*, 109348. https://doi.org/10.1016/j.agrformet.2023.109348

Amna, H., Shahzad, M. K., He, P., & Jiang, L. (2020). Stem taper equations for three major conifer species of Northeast China. *Scandinavian Journal of Forest Research*, *35*(8), 562–576. https://doi.org/10.1080/02827581.2020.1843703

Arellano, G., Zuleta, D., & Davies, S. J. (2021). Tree death and damage: A standardized protocol for frequent surveys in tropical forests. *Journal of Vegetation Science*, *32*(1), 1–14. https://doi.org/10.1111/jvs.12981

Bazezew, M. N., Fehrmann, L., Kleinn, C., & Nölke, N. (2024). Modeling a new taper curve and form factor of tree branches using terrestrial laser scanning. *Forestry: An International Journal of Forest Research*, *97*(1), 1–18. https://doi.org/10.1093/forestry/cpad064

Bazezew, M. N., Griese, N., Fehrmann, L., Kleinn, C., & Nölke, N. (2024). Modeling the horizontal distribution of tree crown biomass from terrestrial laser scanning data. *Science of The Total Environment*, *952*, 175377. https://doi.org/10.1016/j.scitotenv.2024.175377

Bazezew, M. N., Hussin, Y. A., & Kloosterman, E. H. (2018). Integrating airborne LiDAR and terrestrial laser scanner forest parameters for accurate above-ground biomass/carbon estimation in Ayer Hitam tropical forest, Malaysia. *International Journal of Applied Earth Observation and Geoinformation*, *73*, 638–652. https://doi.org/10.1016/j.jag.2018.07.026

Calders, K., Newnham, G., Burt, A., Murphy, S., Raumonen, P., Herold, M., Culvenor, D., Avitabile, V., Disney, M., Armston, J., & Kaasalainen, M. (2015). Nondestructive estimates of above-ground biomass using terrestrial laser scanning. *Methods in Ecology and Evolution*, *6*(2), 198–208. https://doi.org/10.1111/2041-210X.12301

Cao, Q. V. (2009). Calibrating a segmented taper equation with two diameter measurements. *Southern Journal of Applied Forestry*, *33*(2), 58–61. https://doi.org/10.1093/sjaf/33.2.58

CloudCompare. (2024). *CloudCompare software: 3D point cloud and mesh processing project* (Version 2.13.0). https://www.danielgm.net/cc/

Computree. (2024). *Computree: a platform for processing 3D point clouds* (5.3.2). Computree Group. http://rdinnovation.onf.fr/projects/computree/wiki

Craven, P., & Wahba, G. (1978). Smoothing noisy data with spline functions. *Numerische Mathematik*, *31*(4), 377–403. https://doi.org/10.1007/BF01404567

Cyclone Register 360 Plus. (2024). *Cyclone Register 360 Plus: Point cloud registration software. Leica Geosystems AG, 9435 Heerbrugg, Switzerland* (v2024.0.1). Leica Geosystems. https://leica-geosystems.com/en-us/products/laser-scanners/software/leica-cyclone/leica-cyclone-register-360

Dai, W., Yang, B., Liang, X., Dong, Z., Huang, R., Wang, Y., & Li, W. (2019). Automated fusion of forest airborne and terrestrial point clouds through canopy density analysis. *ISPRS Journal of Photogrammetry and Remote Sensing*, *156*, 94–107. https://doi.org/10.1016/j.isprsjprs.2019.08.008

Daryaei, A., & Sohrabi, H. (2016). Additive biomass equations for small diameter trees of temperate mixed deciduous forests. *Scandinavian Journal of Forest Research*, *31*(4), 394–398. https://doi.org/10.1080/02827581.2015.1089932

Dassot, M., Constant, T., & Fournier, M. (2011). The use of terrestrial LiDAR technology in forest science: application fields, benefits and challenges. *Annals of Forest Science*, *68*(5), 959–974. https://doi.org/10.1007/s13595-011-0102-2

Demol, M., Wilkes, P., Raumonen, P., Moorthy, S. M. K., Calders, K., Gielen, B., & Verbeeck, H. (2022). Volumetric overestimation of small branches in 3D reconstructions of Fraxinus excelsior. *Silva Fennica*, *56*(1), 1–26. https://doi.org/10.14214/sf.10550

Farr, G. E. (2019). Binary functions, degeneracy, and alternating dimaps. *Discrete Mathematics*, *342*(5), 1510–1519. https://doi.org/10.1016/j.disc.2019.01.029

Friedman, J. H. (1991). Multivariate adaptive regression splines. *The Annals of Statistics*, *19*(1), 1–67. https://doi.org/10.1214/aos/1176347963

683 Gale, M. G., Cary, G. J., Van Dijk, A. I. J. M., & Yebra, M. (2021). Forest fire fuel through the lens of
684 remote sensing: review of approaches, challenges and future directions in the remote sensing of
685 biotic determinants of fire behaviour. *Remote Sensing of Environment*, *255*, 112282.
686 https://doi.org/10.1016/j.rse.2020.112282
687 Griebel, A., Bennett, L. T., Culvenor, D. S., Newnham, G. J., & Arndt, S. K. (2015). Reliability and
688 limitations of a novel terrestrial laser scanner for daily monitoring of forest canopy dynamics.
689 *Remote Sensing of Environment*, *166*, 205–213. https://doi.org/10.1016/j.rse.2015.06.014
690 Griese, N., Kleinn, C., & Nolke, N. (2025). High terrestrial laser scanning: a new perspective into tree
691 crown characteristics. *Manuscript Submitted for Publication*.
692 Hackenberg, J., Spiecker, H., Calders, K., Disney, M., & Raumonen, P. (2015). SimpleTree —an
693 efficient open source tool to build tree models from TLS clouds. *Forests*, *6*(11), 4245–4294.
694 https://doi.org/10.3390/f6114245
695 Hackenberg, J., Wassenberg, M., Spiecker, H., & Sun, D. (2015). Non destructive method for biomass
696 prediction combining TLS derived tree volume and wood density. *Forests*, *6*(4), 1274–1300.
697 https://doi.org/10.3390/f6041274
698 Hall, J., Muscarella, R., Quebbeman, A., Arellano, G., Thompson, J., Zimmerman, J. K., & Uriarte, M.
699 (2020). Hurricane-induced rainfall is a stronger predictor of tropical forest damage in Puerto Rico
700 than maximum wind speeds. *Scientific Reports*, *10*(1), 4318. https://doi.org/10.1038/s41598-020-
701 61164-2
702 Henrich, J., van Delden, J., Seidel, D., Kneib, T., & Ecker, A. S. (2024). TreeLearn: A deep learning
703 method for segmenting individual trees from ground-based LiDAR forest point clouds. *Ecological*
704 *Informatics*, *84*, 102888. https://doi.org/10.1016/j.ecoinf.2024.102888
705 Hosoi, F., Nakai, Y., & Omasa, K. (2013). 3-D voxel-based solid modeling of a broad-leaved tree for
706 accurate volume estimation using portable scanning lidar. *ISPRS Journal of Photogrammetry and*
707 *Remote Sensing*, *82*, 41–48. https://doi.org/10.1016/j.isprsjprs.2013.04.011
708 ITSMe. (2024). *ITSMe: Individual tree structural metrics* (1.0.0). https://github.com/lmterryn/ITSMe
709 Jiménez, E., Vega, J. A., Ruiz-González, A. D., Guijarro, M., Alvarez-González, J. G., Madrigal, J.,
710 Cuiñas, P., Hernando, C., & Fernández-Alonso, J. M. (2013). Carbon emissions and vertical

pattern of canopy fuel consumption in three Pinus pinaster Ait. active crown fires in Galicia (NW Spain). *Ecological Engineering*, *54*, 202–209. https://doi.org/10.1016/j.ecoleng.2013.01.039

Kershaw, J. A., & Maguire, D. A. (1996). Crown structure in western hemlock, Douglas-fir, and grand fir in western Washington: horizontal distribution of foliage within branches. *Canadian Journal of Forest Research*, *26*(1), 128–142. https://doi.org/10.1139/x26-014

Kleinn, C., Magnussen, S., Nölke, N., Magdon, P., Álvarez-González, J. G., Fehrmann, L., & Pérez-Cruzado, C. (2020). Improving precision of field inventory estimation of aboveground biomass through an alternative view on plot biomass. *Forest Ecosystems*, *7*(1), 57. https://doi.org/10.1186/s40663-020-00268-7

Knapp, N., Fischer, R., & Huth, A. (2018). Linking lidar and forest modeling to assess biomass estimation across scales and disturbance states. *Remote Sensing of Environment*, *205*, 199–209. https://doi.org/10.1016/j.rse.2017.11.018

Knapp, N., Huth, A., & Fischer, R. (2021). Tree crowns cause border effects in area-based biomass estimations from remote sensing. *Remote Sensing*, *13*(8), 1–19. https://doi.org/10.3390/rs13081592

Lau, A., Bentley, L. P., Martius, C., Shenkin, A., Bartholomeus, H., Raumonen, P., Malhi, Y., Jackson, T., & Herold, M. (2018). Quantifying branch architecture of tropical trees using terrestrial LiDAR and 3D modelling. *Trees*, *32*(5), 1219–1231. https://doi.org/10.1007/s00468-018-1704-1

Lau, A., Martius, C., Bartholomeus, H., Shenkin, A., Jackson, T., Malhi, Y., Herold, M., & Bentley, L. P. (2019). Estimating architecture-based metabolic scaling exponents of tropical trees using terrestrial LiDAR and 3D modelling. *Forest Ecology and Management*, *439*, 132–145. https://doi.org/10.1016/j.foreco.2019.02.019

Leica BLK360 G1 Imaging Laser Scanner. (2024). *Leica BLK360 Imaging Laser Scanner. Leica Geosystems, Heerbrugg, Canton of St. Gallen, Switzerland*. https://leica-geosystems.com/

Li, Y., Su, Y., Zhao, X., Yang, M., Hu, T., Zhang, J., Liu, J., Liu, M., & Guo, Q. (2020). Retrieval of tree branch architecture attributes from terrestrial laser scan data using a Laplacian algorithm. *Agricultural and Forest Meteorology*, *284*(11), 107874–107888. https://doi.org/10.1016/j.agrformet.2019.107874

739 Liang, X., Kankare, V., Yu, X., Hyyppä, J., & Holopainen, M. (2014). Automated stem curve
740 measurement using terrestrial laser scanning. *IEEE Transactions on Geoscience and Remote*
741 *Sensing*, *52*(3), 1739–1748. https://doi.org/10.1109/TGRS.2013.2253783
742 LiDARMill. (2023). *LiDARMill: Cloud-based LiDAR post-processing platform. Phoenix LiDAR*
743 *Systems, 2113 Wells Branch Pkwy Ste 4000, Austin, TX 78728, USA* (No. v3). Phoenix LiDAR
744 Systems. https://phoenixlidar.com/lidarmill
745 Lin, L. I.-K. (1989). A concordance correlation coefficient to evaluate reproducibility. *Biometrics*,
746 *45*(1), 255–268. https://doi.org/10.2307/2532051
747 Lindberg, E., Holmgren, J., Olofsson, K., & Olsson, H. (2012). Estimation of stem attributes using a
748 combination of terrestrial and airborne laser scanning. *European Journal of Forest Research*,
749 *131*(6), 1917–1931. https://doi.org/10.1007/s10342-012-0642-5
750 MacFarlane, D. W. (2020). Functional relationships between branch and stem wood density for
751 temperate tree species in North America. *Frontiers in Forests and Global Change*, *3*, 63.
752 https://doi.org/10.3389/ffgc.2020.00063
753 Mascaro, J., Detto, M., Asner, G. P., & Muller-Landau, H. C. (2011). Evaluating uncertainty in mapping
754 forest carbon with airborne LiDAR. *Remote Sensing of Environment*, *115*(12), 3770–3774.
755 https://doi.org/10.1016/j.rse.2011.07.019
756 Milborrow, S. (2021). *earth: Multivariate adaptive regression splines* (5.3.4). R Foundation for
757 Statistical Computing. https://cran.r-project.org/package=earth
758 Ojoatre, S., Zhang, C., Hussin, Y. A., Kloosterman, H. E., & Ismail, M. H. (2019). Assessing the
759 uncertainty of tree height and aboveground biomass from terrestrial laser scanner and hypsometer
760 using airborne LiDAR data in tropical rainforests. *IEEE Journal of Selected Topics in Applied*
761 *Earth Observations and Remote Sensing*, *12*(10), 4149–4159. https://doi.org/10.1109/JSTARS
762 .2019.2944779
763 Panagiotidis, D., Abdollahnejad, A., & Slavík, M. (2022). 3D point cloud fusion from UAV and TLS
764 to assess temperate managed forest structures. *International Journal of Applied Earth Observation*
765 *and Geoinformation*, *112*, 102917. https://doi.org/10.1016/j.jag.2022.102917
766 Pérez-Cruzado, C., Kleinn, C., Magdon, P., Álvarez-González, J. G., Magnussen, S., Fehrmann, L., &

Nölke, N. (2021). The horizontal distribution of branch biomass in European beech: a model based on measurements and TLS based proxies. *Remote Sensing*, *13*(5), 1–15. https://doi.org/10.3390/rs13051041

Pitkänen, T. P., Raumonen, P., Liang, X., Lehtomäki, M., & Kangas, A. (2021). Improving TLS-based stem volume estimates by field measurements. *Computers and Electronics in Agriculture*, *180*, 105882. https://doi.org/10.1016/j.compag.2020.105882

Qi, Y., Coops, N. C., Daniels, L. D., & Butson, C. R. (2022). Comparing tree attributes derived from quantitative structure models based on drone and mobile laser scanning point clouds across varying canopy cover conditions. *ISPRS Journal of Photogrammetry and Remote Sensing*, *192*, 49–65. https://doi.org/10.1016/j.isprsjprs.2022.07.021

R Core Team. (2024). *R: A language and environment for statistical computing. R foundation for statistical computing* (R-4.4.2). R Foundation for Statistical Computing. https://www.r-project.org/

Raumonen, P., Kaasalainen, M., Åkerblom, M., Kaasalainen, S., Kaartinen, H., Vastaranta, M., Holopainen, M., Disney, M., & Lewis, P. (2013). Fast automatic precision tree models from terrestrial laser scanner data. *Remote Sensing*, *5*(2), 491–520. https://doi.org/10.3390/rs5020491

RECON-XT LiDAR. (2024). *UAV-based laser scanner: RECON-XT LiDAR sensor. Phoenix LiDAR Systems, 2113 Wells Branch Pkwy Ste 4000, Austin, TX 78728, USA*. https://phoenixlidar.com/recon-xt/#key-features-section

Roussel, J.-R., Auty, D., De Boissieu, F., & Meador, A. S. (2024). *lidR: Airborne LiDAR data manipulation and visualization for forestry applications*. https://cran.r-project.org/web/packages/lidR/lidR.pdf

Salekin, S., Catalán, C. H., Boczniewicz, D., Phiri, D., Morgenroth, J., Meason, D. F., & Mason, E. G. (2021). Global tree taper modelling: A review of applications, methods, functions, and their parameters. *Forests*, *12*(7), 1–20. https://doi.org/10.3390/f12070913

SimpleForest. (2024). *SimpleForest: a 3D tree modelling software from point cloud data* (5.3.2). https://www.simpleforest.org/

Singh, K. K., Chen, G., McCarter, J. B., & Meentemeyer, R. K. (2015). Effects of LiDAR point density

and landscape context on estimates of urban forest biomass. *ISPRS Journal of Photogrammetry and Remote Sensing*, *101*, 310–322. https://doi.org/10.1016/j.isprsjprs.2014.12.021

Srinivasan, S., Popescu, S. C., Eriksson, M., Sheridan, R. D., & Ku, N.-W. (2015). Terrestrial laser scanning as an effective tool to retrieve tree level height, crown Width, and stem diameter. *Remote Sensing*, *7*(2), 1877–1896. https://doi.org/10.3390/rs70201877

Tahvanainen, T., & Forss, E. (2008). Individual tree models for the crown biomass distribution of Scots pine, Norway spruce and birch in Finland. *Forest Ecology and Management*, *255*(3), 455–467. https://doi.org/10.1016/j.foreco.2007.09.035

Terryn, L., Calders, K., Åkerblom, M., Bartholomeus, H., Disney, M., Levick, S., Origo, N., Raumonen, P., & Verbeeck, H. (2023). Analysing individual 3D tree structure using the R package ITSMe. *Methods in Ecology and Evolution*, *14*(1), 231–241. https://doi.org/10.1111/2041-210X.14026

Terryn, L., Calders, K., Bartholomeus, H., Bartolo, R. E., Brede, B., D'hont, B., Disney, M., Herold, M., Lau, A., Shenkin, A., Whiteside, T. G., Wilkes, P., & Verbeeck, H. (2022). Quantifying tropical forest structure through terrestrial and UAV laser scanning fusion in Australian rainforests. *Remote Sensing of Environment*, *271*, 112912. https://doi.org/10.1016/j.rse.2022.112912

Torr, P. H. S., & Zisserman, A. (2000). MLESAC: A new robust estimator with application to estimating image geometry. *Computer Vision and Image Understanding*, *78*(1), 138–156. https://doi.org/10.1006/cviu.1999.0832

TreeLearn. (2024). *TreeLearn: A deep learning method for segmenting individual trees from ground-based LiDAR forest point clouds* (1.2). GitHub. https://doi.org/10.1016/j.ecoinf.2024.102888

Vaaja, M. T., Virtanen, J.-P., Kurkela, M., Lehtola, V., Hyyppä, J., & Hyyppä, H. (2016). The fffect of wind on tree stem parameter estimation using terrestrial laser scanning. *ISPRS Annals of Photogrammetry, Remote Sensing and Spatial Information Sciences*, *III–8*(July), 117–122. https://doi.org/10.5194/isprsannals-iii-8-117-2016

Ver Planck, N. R., & MacFarlane, D. W. (2014). Modelling vertical allocation of tree stem and branch volume for hardwoods. *Forestry: An International Journal of Forest Research*, *87*(3), 459–469. https://doi.org/10.1093/forestry/cpu007

Weiser, H., Schäfer, J., Winiwarter, L., Krašovec, N., Fassnacht, F. E., & Höfle, B. (2022). Individual tree point clouds and tree measurements from multi-platform laser scanning in German forests. *Earth System Science Data*, *14*(7), 2989–3012. https://doi.org/10.5194/essd-14-2989-2022

Wilkes, P., Lau, A., Disney, M., Calders, K., Burt, A., Gonzalez de Tanago, J., Bartholomeus, H., Brede, B., & Herold, M. (2017). Data acquisition considerations for Terrestrial Laser Scanning of forest plots. *Remote Sensing of Environment*, *196*, 140–153. https://doi.org/10.1016/j.rse.2017.04.030

Xu, M., & Harrington, T. B. (1998). Foliage biomass distribution of loblolly pine as affected by tree dominance, crown size, and stand characteristics. *Canadian Journal of Forest Research*, *28*(6), 887–892. https://doi.org/10.1139/x98-060

Zhou, R., Sun, H., Ma, K., Tang, J., Chen, S., Fu, L., & Liu, Q. (2023). Improving estimation of tree parameters by fusing ALS and TLS point cloud data based on canopy gap shape featurepoints. *Drones*, *7*(8). https://doi.org/10.3390/drones7080524

Zuleta, D., Krishna Moorthy, S. M., Arellano, G., Verbeeck, H., & Davies, S. J. (2022). Vertical distribution of trunk and crown volume in tropical trees. *Forest Ecology and Management*, *508*, 120056. https://doi.org/10.1016/j.foreco.2022.120056